Ocean Engineering 319 (2025) 120262

Contents lists available at ScienceDirect

Ocean Engineering

journal homepage: www.elsevier.com/locate/oceaneng

Research paper

Dynamic analysis of crane barge during vibratory extraction of offshore monopile foundation

Soheil Salahshour [a,*], Zhiyu Jiang [b], Muk Chen Ong [a], Bjørn Skaare [a,c]

[a] *Department of Mechanical and Structural Engineering and Materials Science, University of Stavanger, Stavanger, Norway*
[b] *Department of Engineering Sciences, University of Agder, Grimstad, Norway*
[c] *Equinor ASA, Norway*

ARTICLE INFO

Keywords:
Vibratory extraction
Monopile
Soil resistance
Crane barge
Time-domain simulations

ABSTRACT

As offshore wind turbines approach the end of their operational lifespan, the decommissioning process is gaining increasing importance, which highlights the need to develop expertise in the marine operations involved in this task. This study focuses on simulating the vibratory extraction of a monopile foundation for an offshore wind turbine using a crane barge. A numerical model is developed to couple the dynamic behavior of the monopile with that of the barge. To accurately represent soil behavior during the extraction process, a high-fidelity finite element model is first established to calculate the soil resistance component under high-frequency cyclic loading generated by the vibro-hammer. Then, time domain numerical simulations of the monopile decommissioning process are carried out, and an external Dynamic Link Library (DLL) is developed to integrate this soil resistance force into the time-domain program. Additionally, the centrifugal force exerted by the vibro-hammer is incorporated into the model through a separate DLL. Time-domain simulations are performed to analyze the barge's motion and the tension in the lifting wire under calm water conditions. These results are then compared with simulations conducted under long-crested waves to provide a comprehensive understanding of the extraction process. This study also examines the effect of the dynamic positioning system on the barge's dynamic response and the tension in the lifting wire. The outcome of this paper contributes to a better understanding of the complex decommissioning process under marine environments.

1. Introduction

Marine operations for offshore wind can be classified to three main categories consisting of (a) transportation, (b) installation, (c) maintenance, and (d) decommissioning. The subject of decommissioning of offshore wind is new as many of the installed offshore wind turbines (OWTs) are approaching the end of their design lifetime of 20–25 years. Understanding and optimizing the extraction of offshore monopiles from the seabed in decommissioning operations give both environmental benefits and cost reduction. Monopile foundation is the dominant type that is used in 81.2% of OWTs in Europe (Komusanac et al., 2022). The current practice of removal of monopiles which is cutting near or below the seabed level is time-consuming. Although ongoing research aims to reduce cutting time, uncertainties surrounding subsea operations pose challenges for this method. An alternative method, successfully employed in decommissioning of the Lely wind farm, involves using a vibro-hammer to extract the monopile entirely. The method has proved to significantly reduce operation time. Numerical study conducted by Salahshour et al. (2023) indicated that vibratory extraction is highly effective in sandy seabed conditions, but less so in clayey seabed (Salahshour et al., 2024). Therefore, this study aims to illuminate the process of monopile foundation removal from dense sand seabed condition and provide insights for operators and engineers in the field.

The results of study on evaluating risks in decommissioning reveal that the lifting and loading are the most safety-critical operations during this phase (Shafiee and Adedipe, 2022). It is important for asset managers to mitigate the risks related to the removal of wind turbines, vessel accessibility and operational efficiency, whilst ensuring high safety practices. Hence, numerical modeling tools offer a valuable advantage by providing operators with insights to mitigate the risks of unforeseen events during decommissioning operations.

The success of numerical simulation in lifting operation depends on accurate definition of the hoisting system (the stiffness of the crane, the wire and the damping coefficients), selection of the hydrodynamic

* Corresponding author.
E-mail address: soheil.salahshourlangeroodi@uis.no (S. Salahshour).

https://doi.org/10.1016/j.oceaneng.2024.120262
Received 31 October 2024; Received in revised form 8 December 2024; Accepted 27 December 2024

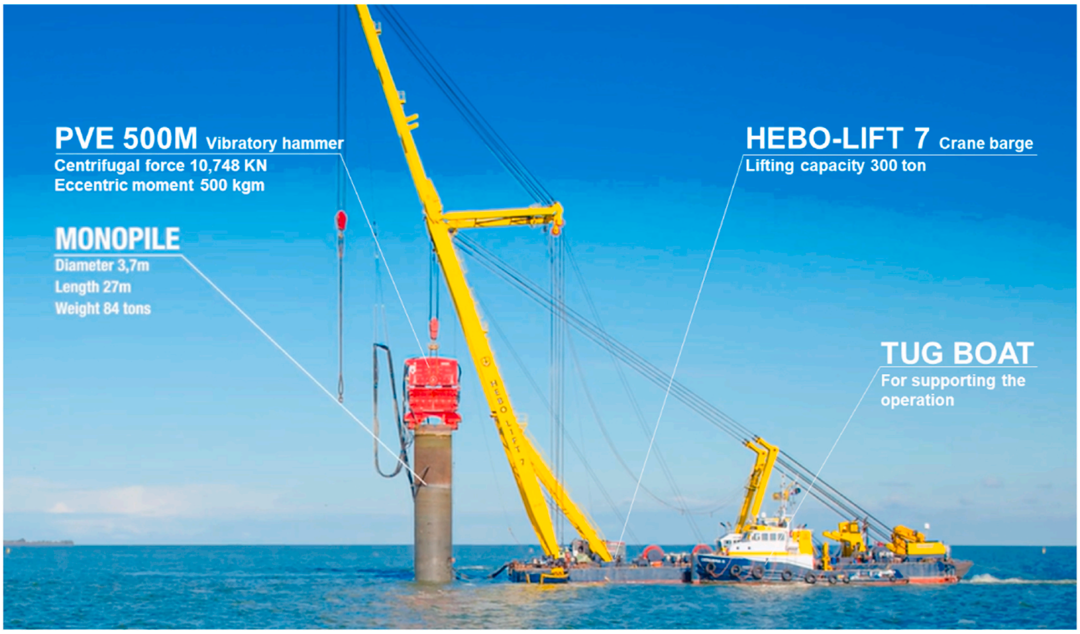

Fig. 1. System of monopile & vibro-hammer in decommissioning of Lely wind park (Dieseko Group, 2017).

coefficients for the structure, extreme value estimation of the dynamic analysis results and selection of the acceptance criteria (Gordon et al., 2013). However, in this study the lifting crane is modeled as a rigid object connected to the crane barge since the main goal of the analysis is the dynamic response of the barge itself when it is exposed to external loads. Extreme value estimation and workability of the barge can be the subject of another study.

The subjects of installation of the OWT's foundation and top parts have been studied in the literature. A comprehensive summary of installation modelling with focus on lowering through the wave splash zone, fully submerged, and when the structure approaches the seabed is done by de Andrade et al. (2023). The lowering mechanism of foundations presents a complex engineering challenge, necessitating the use of time-domain simulation for offshore operations. Gordon et al. (2013) conducted time domain modeling procedure for suction pile lowering through the splash zone. They specifically addressed pile lowering from a relatively small installation vessel with the pile oriented with its long axis nearly parallel to the water surface. Their model consists of time domain simulation consisting of the crane, wire, sling and pile system. This system was subjected to vessel motions at the crane tip, hydrodynamic loading on the pile, and pile flooding. They also described the sensitivity of winch wire tension to sea-state, lowering velocity and hydrodynamic model coefficients, and suction pile characteristics. Dynamic responses of a heavy steel cylinder hanged by a large floating crane in the process of immersing into waves were studied experimentally and numerically by Chen et al. (2014). Li et al. (2015b) addressed numerical modeling and time-domain simulations of the lowering operation for installation of an offshore wind turbine monopile with a diameter of 5.7 m and examined the nonstationary dynamic responses of the lifting system in irregular waves. In another study, Li et al. (2015a) utilized a time-domain simulation approach, employing a dynamic link library (DLL), to investigate the impact of vessel-shielding effects on the lowering operations of monopile and jacket foundations for offshore wind turbines. Similarly, Zhu et al. (2017) explored the responses and permissible sea states for static and dynamic lowering processes of tripod foundations, affirming the necessity of time-domain simulation for such scenarios. Zhang et al. (2022b) delved into the dynamic characteristics of vessel-three-bucket jacket foundation lifting systems during the lowering process, combining frequency domain hydrodynamic calculations with time-domain simulation to assess operation feasibility in specific sea conditions. Key concerns, such as slamming load, lowering speed, and added mass variation for bucket jackets, have also been addressed (Van Doorn, 2016; Zhang et al., 2022a).

Mitigating offshore operation risks hinges on robust risk management during planning and design stages. Acero et al. (2016b) introduced a comprehensive method based on extreme marine parameters, applicable to various offshore operations influenced by environmental factors. Assessing permissible sea states entails defining critical events and their associated parameters, followed by evaluating extreme responses, both requiring extensive dynamic response analysis through numerical simulations. Zhao et al. (2018) simulated single-blade OWT installations, evaluating extreme values using the mean up-crossing rate method and Poisson probability distribution. Frequency spectrum analysis is employed for extreme value determination in OWT operation and maintenance (Li et al., 2022). Furthermore, time-domain simulation and extreme value distribution models are utilized in offshore piling (Li et al., 2016) and OWT installations (Acero et al., 2016a). Chen et al. (2022) studied the dynamic responses of a four-pile jacket foundation lowering system under different random wave actions and established a method to define the extreme response and the allowable sea state, which has been rarely discussed in the installation of jacket foundations of OWTs. In another research, Chen et al. (2024) conducted an analysis of lift-off operation of the jacket foundation from a transportation barge by including the hydrodynamic interaction in a multi-body system and they investigated the operability of the lift-off operation in certain sea area. Hong et al. (2022) provided a new onsite installation concept for floating OWTs where a catamaran and spar are mechanically connected, and one of the wind turbines is lifted, waiting for mating operation. The proposed novel mechanical coupling using a fender system was applied to connect the vessel and the substructure to increase the operability of the installation operation. In another study for the same installation method, Hong et al. (2023) put the focus on features such as viscous drag on the spar, hydrodynamic interaction between floating bodies, long- and short-crested waves, first- and second-order wave loads, wave directions, and wave peak periods. Additionally, they provided an estimation of weather window for installation operability. Gao et al. (2023) presented an innovative concept for pre-assembled OWTs that is tentatively designed for median or large water-depth sites. This method requires the floating foundation to be already installed on the site. The conventional jacked-up installation vessel is replaced by a small

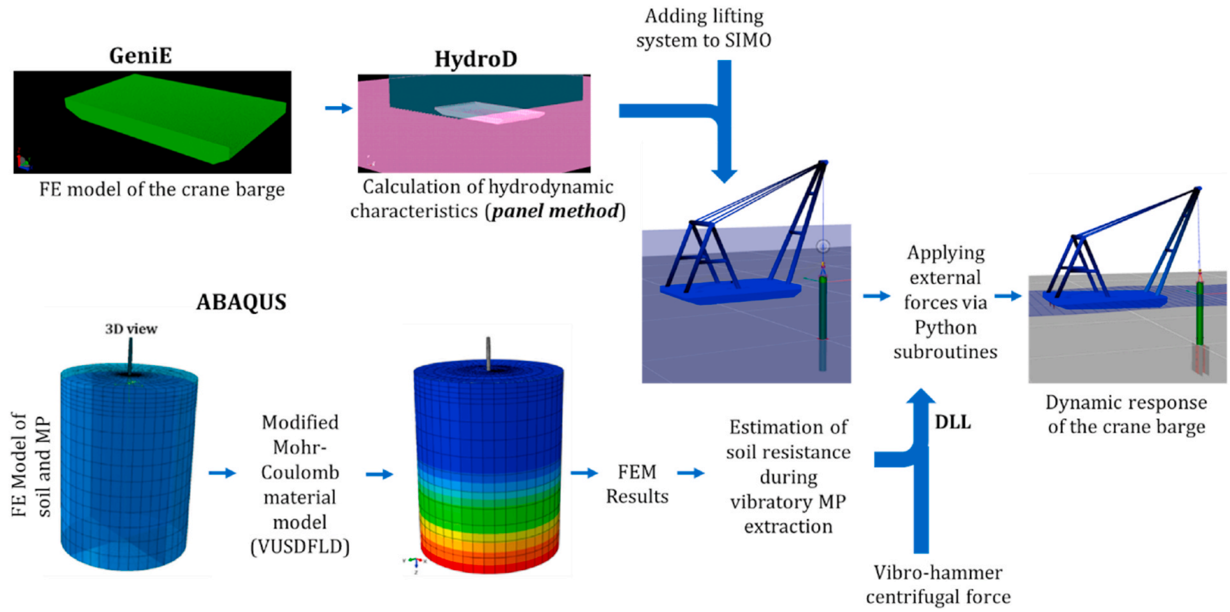

Fig. 2. Visual presentation of this study.

waterplane area twin-hull vessel (SWATH) equipped with the dynamic position (DP) system, and the heavy lifting is replaced by the low-height lifting crane with lifting wires for lowering the assembled OWT to the floating foundation.

For the phase of maintenance/operation of the OWTs, Deng et al., 2023 performed both experimental measurements and numerical prediction of the dynamic tension in the umbilical during launch and recovery of remotely operated underwater vehicle (ROV), while passing through the wave splash zone. They carried out a coupled vessel, umbilical and ROV hydrodynamic analysis for launching and recovering of ROV with coupling characteristics being examined.

Decommissioning is the final phase in the lifetime of OWTs and is inevitable. One of the most challenging tasks during this phase is the removal of the foundation. An example of this operation is shown in Fig. 1. Over 80% of bottom-fixed OWTs in Europe utilize monopile foundations (Komusanac et al., 2022). Monopile removal from the seabed can be carried out through either partial or complete removal (Salahshour et al., 2022). Complete removal is the more sustainable and environmentally friendly option, as no portion of the monopile is left in the seabed, and the retrieved steel can be recycled, reducing the carbon footprint compared to the production of new steel. The global simulation of monopile extraction, including pile-soil interaction, has not been studied. Given the large number of OWTs approaching decommissioning, there is an obvious need to develop expertise and knowledge in this area.

The complete extraction of offshore monopile foundations using vibratory hammers offers significant economic and environmental advantages compared to conventional removal methods. From an economic perspective, vibratory extraction is substantially faster than traditional cutting methods, reducing the operational duration and associated costs. Additionally, this method allows the retrieved steel to be recycled, rather than left abandoned in the seabed, providing a valuable material resource.

Environmentally, offshore wind sites represent unique locations with high potential for harnessing renewable energy. Ensuring the sustainability and reusability of these sites is essential for future applications. Complete monopile removal aligns with this objective, whereas partial removal through cutting often leaves residual structures that may compromise site reusability. Furthermore, recycling the retrieved steel as secondary steel is associated with significantly lower carbon emissions compared to the production of primary steel, further enhancing the environmental benefits of vibratory extraction. Partial removal methods typically require excavation or dredging within or outside the monopile to reach the desired cutting depth (Hinzmann et al., 2020, 2021; Salahshour et al., 2023). This process can negatively impact the marine ecosystem at the site. In contrast, vibratory extraction minimizes seabed disturbance, thereby reducing its ecological footprint.

For the simulations conducted in this study, a crane barge is employed as the lifting vessel. This choice offers a lower day-rate compared to heavy lift or jack-up vessels, making it a cost-effective alternative. The modeled crane barge is equipped with bow and stern thrusters, enabling linear motion and enhancing its maneuverability during the monopile extraction process. The focus of this study is extraction of the monopile from the seabed to assess how the monopile and hammer weights, soil resistance, and centrifugal force of the vibro-hammer influence on dynamic response of the crane barge. This study introduces a novel approach by incorporating soil resistance under cyclic loading and the vibro-hammer's centrifugal force through a Dynamic Link Library (DLL). The dynamic response analysis in this study is performed using SIMA, a workbench developed by SINTEF and widely recognized for its robust capabilities in simulating marine operations. However, SIMA exhibits certain limitations in modeling soil behavior. To address these constraints, the pile-soil interaction analysis has been conducted using ABAQUS, as detailed in Salahshour et al. (2023). The results from the ABAQUS simulations are incorporated into the present study to enhance the accuracy and comprehensiveness of the analysis. This implementation enables a more accurate and realistic simulation of the vibratory monopile extraction process, enhancing predictive capability and offering deeper insights into marine operation for monopile removal. The structure of this paper is as follows: Section 2 provides a detailed description of the modeling of the coupled system comprising the barge, monopile, hook, and lifting wire. In Section 3, the model is developed by analyzing the effects of the vibro-hammer's centrifugal force and soil resistance, as well as their combined influence, to simulate the vibratory monopile extraction process. Section 4 examines the dynamic response of the crane barge under two distinct sea states. Finally, concluding remarks are presented in Section 5.

2. Modeling of the coupled system

The removal of an offshore monopile foundation using vibro-hammer includes several steps: (1) positioning of the floater, (2)

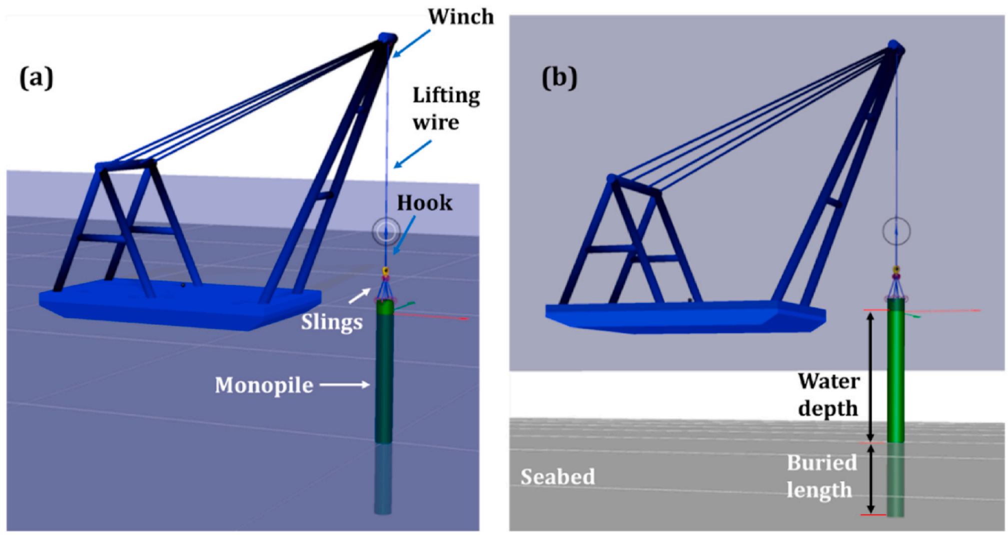

Fig. 3. Lifting system arrangement (a) isometric view (b) below water surface.

mounting vibro-hammer on top of the monopile, (3) extracting from seabed, (4) passing splash zone, (5) hanging in air, and (6) down-ending on deck. In this research, only Step 3 is the subject of study.

2.1. General procedure

This section outlines the methodologies and tools employed for numerically modeling the vibratory monopile extraction method. The Sesam package, developed by SINTEF Ocean (2022), serves as the primary tool for this study. Panel models for the crane barge are generated using GeniE, a conceptual Finite Element Method (FEM) modeling and analysis program integrated into the Sesam package. These panel models are then employed in HydroD for hydrodynamic modeling and calculation. The mass properties for the crane barge hydrodynamic model were estimated under heavy loading conditions.

The hydrodynamic coefficients, including hydrostatic stiffness, added mass, radiation damping, and transfer functions, are calculated in the frequency domain in HydroD using WADAM analysis based on the potential flow theory, and results are subsequently imported into SIMA. SIMA is a workbench in Sesam package, to generate rigid body models of both the crane barge and the monopile using SIMO. SIMO serves as a time-domain simulation tool tailored for examining the dynamics of multi-body systems and station-keeping. A visual presentation of the steps implemented in this study is illustrated in Fig. 2. It is worth mentioning that wind and current forces are not included in this study and only the wave excitation force is included in simulations.

As depicted in Fig. 2, a DLL is utilized to implement soil resistance and vibro-hammer centrifugal force. A DLL is a compiled library file containing reusable functions and data, enabling multiple programs to access them concurrently (Microsoft documentation). While DLLs are primarily associated with Windows environments, their functionality has counterparts in other systems, such as shared libraries in Linux. To integrate a DLL with software, it must be loaded either at runtime or during the compilation process (Microsoft documentation). To effectively use a DLL, the application must declare the function prototypes of the functions it intends to access. Once the DLL is loaded, its functions can be invoked as if they are part of the application itself. The workflow for implementing a DLL integration generally includes the following steps.

- Exporting Functions from the DLL,
- Loading the DLL in the Software,
- Interfacing with the DLL,
- Data Exchange.

Table 1
Main parameters of the crane barge.

Vessel	Unit	Value
Length O.A.	[m]	60
Length B.P.	[m]	60
Breadth	[m]	33
Depth	[m]	5.5
Draught	[m]	3.6
Displacement	[tons]	6810
Metacentric height	[m]	22
Roll period	[s]	7.5
Pitch period	[s]	8.2
Heave period	[s]	7.1

SINTEF has developed the SimoPy utility, a Python interface for defining custom body forces in SIMO simulations (GitHub - SINTEF/-simapy). This utility enables the implementation of a Python subroutine to model prescribed forces and calculate their effects dynamically and statically within a simulation. The implementation process involves the following steps.

1. **Initialization**: Recognizes and initializes the model and force parameters necessary for the simulation.
2. **Static Force Computation**: Specifies external forces to be applied when the system is in static equilibrium.
3. **Time Step Update**: Updates the simulation time to reflect the progression of the analysis.
4. **Dynamic Force Computation**: Calculates time-dependent forces during the dynamic phase of the simulation.

2.2. Crane barge

The selected floater for the vibratory extraction of the monopile is a crane barge (shown in Fig. 3). The floater utilized in this study is generated based on an existing crane barge currently in service for marine operations. Table 1 presents the primary dimensions of this crane barge, which is equipped with a crane capable of lifting loads of up to 785 tons with an outreach of 25 *m* and a lifting height limit of 60 *m*, the crane barge is well-suited for the task. The crane modeled in this study is assumed to be rigidly attached to the barge's deck. In practice, this crane can rotate about its base, enabling it to extend their reach to longer distances. The flexibility of the crane introduces additional stiffness to the lifting system, which could influence the dynamic response. However, this effect has been excluded from the scope of the

Table 2
Wavelength for operational peak periods.

T_p [s]	5	6	8	10	12
λ [m]	39.04	56.09	96.08	137.32	177.06

present analysis to simplify the modeling.

The reference barge is equipped with both bow and aft thrusters. These thrusters enable linear movement in both forward and astern directions and are considered in the modeling. The crane is rigidly connected to the barge's deck and therefore, its deformations are neglected in this study. The crane barge's shallow draft and high lifting capacity facilitate lifting operations in shallow waters.

Considering the hydrodynamic interaction between two closely positioned floaters is crucial for response estimation (Baar et al., 1992). However, the relatively small size of the monopile in comparison to the floater means the hydrodynamic effects exerted by the monopile on the floater are negligible and can be disregarded (Li et al., 2014). Moreover, the monopile is not floating throughout the extraction process as it is restricted by the surrounding seabed soil. The occurrence of wave diffraction caused by the presence of the monopile is negligible if the incident wave's length (λ) exceeds 5 times the diameter (D) of the monopile, i.e., $\lambda > 5D$. The wavelength of linear waves can be estimated based on the water depth, h, and the wave peak period, T, using the following equation:

$$\lambda = T\sqrt{\frac{g}{k}\tanh\left(k.h\right)} \tag{1}$$

where k is wave number ($k = 2\pi\lambda^{-1}$) and g is gravitational acceleration. For the water depth considered in this study (30 m), the wavelengths are calculated for various peak periods and summarized in Table 2. The wavelengths for operational range of peak periods are larger than $5D = 20\,m$, indicating that diffraction effects can be ignored.

The global coordinate system is established as a right-handed system with the following orientation: the X-axis extends towards the bow, the Y-axis extends towards the port side, and the Z-axis extends upward. The origin of this system is positioned at the center of the monopile, at the level of still water.

The Response Amplitude Operator (RAO) is a fundamental concept in offshore engineering used to describe the dynamic behavior of floating structures when subjected to external loading, such as wave load. RAOs are used to predict how the structure will respond to different wave frequencies and amplitudes.

2.3. System of monopile and vibro-hammer

The monopile considered in this study is modeled based on the one used in field measurements conducted by van Dorp et al. (2021) and has been modeled by Salahshour et al. (2023) to estimate seabed sandy soil resistance while exposed to vibratory loading. However, minor changes have been applied to the monopile's geometry. While maintaining its outer diameter at 4 m and weight at 301 tons, its length has been reduced to 50 m by neglecting the conical part at head of the original monopile and employing a wall thickness of 62 mm. The embedded length of the monopile is 17 m, similar to the previous studies. The considered water depth is equal to 30 m in this study.

A vibratory hammer, known as vibro-hammer, is construction equipment used to drive or extract piles by transmitting high-frequency vibration energy to the pile, which results in loosening surrounding soil particles and reducing resistance. Types include excavator-mounted, crane-suspended, and variable-moment vibro-hammers, chosen based on pile size, weight, and soil conditions. Compared to traditional pile drivers, vibro-hammers offer numerous advantages, such as faster pile driving and extraction, quieter operation, environmental friendliness, and suitability for underwater use. Some models allow full control of vibration.

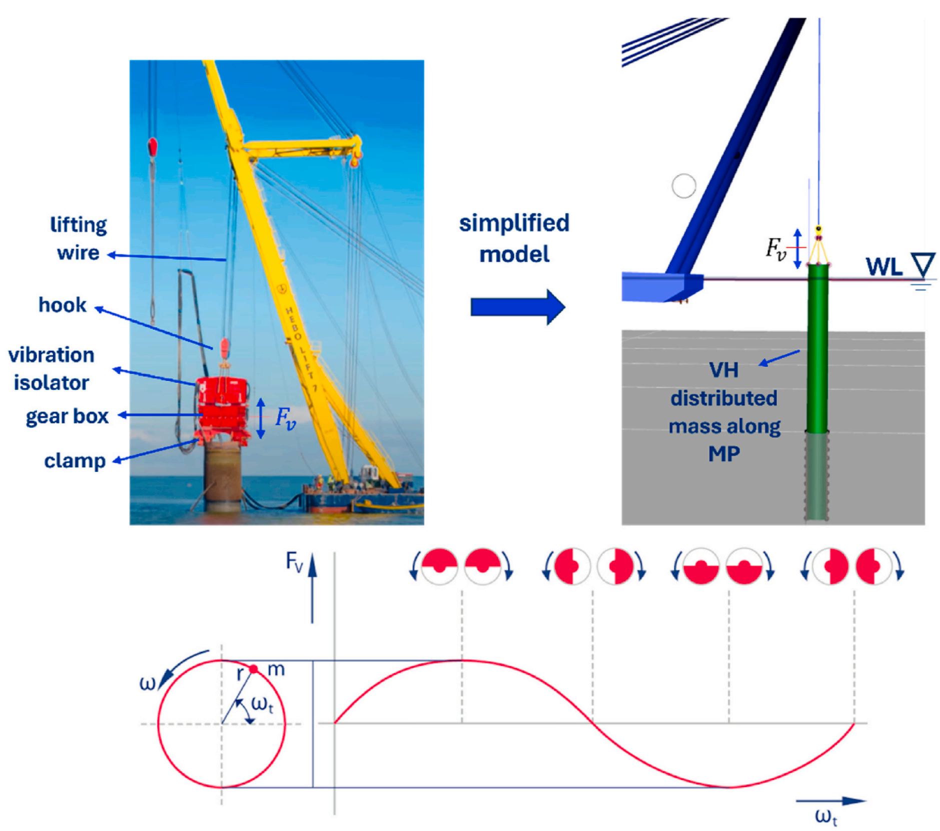

Fig. 4. Numerical modeling simplification for vibro-hammer.

For marine applications, the crane-suspended or free-hanging type of vibro-hammer is commonly employed. During pile driving, the high-frequency oscillations induce liquefaction or degradation in the soil skeleton, thereby reducing soil resistance. The vibro-hammer's weight, combined with the monopile's weight, drives the monopile into the soil until an equilibrium between driving and resisting forces is reached. In vibratory pile extraction, the vibro-hammer initially operates freely for a short period of time. Once the first movement of the pile is observed, the crane uplift force is applied via lifting wire. During extraction process, this force must surpass the combined weight of the vibro-hammer and monopile, as well as the reduced soil resistance. In vibratory extraction, the vibro-hammer is affixed to the top head of the monopile via a hydraulic clamping system. The jaws of the clamp with hardened teeth create a rigid connection. Due to this rigid connection, a simplification is applied to the numerical model where the system of the monopile and vibro-hammer is treated as monopile alone, with the weight of the vibro-hammer and clamping system added to it (as shown in Fig. 4).

In Fig. 4, F_v represents the vertical component of the vibro-hammer centrifugal force, generated by the rotation of eccentric masses (m) with an eccentric radius (r) and a rotational frequency (ω) (Salahshour et al., 2023). ω_t is angular frequency for 2π radians. In this study, the vibro-hammer under consideration has the capability to generate a 640 kgm eccentric moment, able to generate centrifugal force of 13.7 MN at maximum vibration frequency of 23.3 Hz. The weight of this vibro-hammer combined with clamps is assumed to be 105 *tons*. Thus, the weight of the lifting object is considered 406 *tons* in this study.

Gravity and buoyancy forces act on the monopile. As shown in Section 2.2, the monopile's diameter is relatively small compared to the wavelength, and the wave height to structure diameter ratio is low. Since the monopile is modeled as a rigid body, an additional slender element is included to create the viscous effect on the submerged part of it. A drag coefficient of 0.9 is applied to estimate the transverse viscous force based on DNV recommendation. The velocity of water flow varies with depth, being higher near the water surface and decreasing closer to the seabed. This variation results in differing drag coefficients along the monopile, with higher values near the surface and lower values near the seabed. To simplify the analysis, an average drag coefficient has been adopted. The viscous drag per unit length of the monopile is estimated using Morison's equation (Hong et al., 2022):

$$dF_j^{drag} = \frac{1}{2}\rho_w C_d D\left(\dot{u}_w(t) - \dot{u}_p(t)\right)\left|\dot{u}_w(t) - \dot{u}_p(t)\right|dz \tag{2}$$

where ρ_w is the density of the water, C_d is the quadratic drag coefficient, and D is the diameter of each monopile strip cross-section. $\dot{u}_w$ and $\dot{u}_p$ are the velocities of the wave particles and the monopile, respectively. The inertia force on the monopile is dominant force which can be calculated by the following equation:

$$dF_j^{inertia} = \rho_w \frac{\pi D^2}{4} C_M \ddot{u}_w dz - \rho_w \frac{\pi D^2}{4}(C_M - 1)\ddot{u}_b dz \tag{3}$$

where C_M is the inertia coefficient, equal to C_a +1. C_a is added mass coefficient. $\ddot{u}_w$ and $\ddot{u}_p$ are the accelerations of the wave particles and the monopile, respectively. The monopile is a hollow thin cylinder with its top and bottom ends above the water and below the seabed level, respectively. The monopile is filled with water (up to mean sea level), resembling a solid cylinder. Therefore, the added mass coefficients in lateral directions are considered $C_a = 1$. However, it is important to note that as the monopile is gradually extracted from the seabed, its rigidity changes until it is totally detached from the seabed and becomes free. As mentioned in the Introduction section, only extraction from seabed is scope of this study until the bottom end of the monopile is released.

Table 3
Lifting wire and slings properties.

Mode	Unstretched length [m]	Stiffness [N/m]	Damping [N. s/m]	Cross section stiffness [N/m]
Lifting wire	49.25	1.33e-7	3.00e7	1.62e10
Slings	5.57	1.33e-7	2.50e6	1.00e8

2.4. Lifting system

The lifting system for the monopile extraction operation includes hook, crane lift wire, slings, and winch, as shown in Fig. 3. The winch system is modeled at the top of the crane and is 60 m above the sea level. A hook is generally used to connect the lift wire and the slings which are attached to the monopile. Because of the large wight of the monopile, four slings are considered. The main lifting wire and slings properties are provided in Table 3.

The extraction process simulated in this study mirrors the field measurements conducted by van Dorp et al. (2021) and the numerical study by Salahshour et al. (2023). In these studies, a 4 m diameter monopile with embedded length of 17 m was extracted from the seabed within a timeframe of 7 min. The extraction speed of 40.5 mm/s was constant throughout all simulations and was applied to the winch for lifting.

2.5. Eigen value analysis

The natural periods and eigenvectors for selected modes are determined using a linearized system model (SIMA Documentation). The analysis involves constructing mass and stiffness matrices and solving the system using a standard Jacobian solver. Notably, the effects of damping are excluded from this analysis. The mass matrix is derived from the virtual mass matrix, which incorporates both structural and hydrodynamic mass. However, the frequency dependency of the hydrodynamic mass is not considered, as asymptotic values are used for the analysis. Eigen value analysis is performed in the frequency domain to examine the eigen periods of the rigid body motions in the lifting system. The natural modes and corresponding periods are determined by solving Eq (4).

$$\left[-\omega^2(\boldsymbol{M}+\boldsymbol{A})+\boldsymbol{K}\right].\boldsymbol{x}=0 \tag{4}$$

where $\boldsymbol{M}$ represents the mass matrix of the crane barge, the monopile, and the hook while $\boldsymbol{A}$ is the added mass matrix of the crane barge and the monopile, with the added mass at infinite frequency. The total restoring stiffness matrix, $\boldsymbol{K}$, consists of two components: hydrostatic restoring and coupling between the crane barge and the monopile, including wire coupling. The eigenvector $\boldsymbol{x}$ represents the rigid body motions, encompassing 15 degrees of freedom (DOFs) including 6 DOFs for the crane barge and monopile and 3 translational DOFs for hook. The eigenvalues of the crane barge alone, the monopile alone, and the coupled system are analyzed. Tables 4 and 5 present the natural periods and modes of the crane barge and the monopile, highlighting the predominant rigid body motions. To obtain the eigenvalues of the monopile, the crane barge and hook are assumed to be fixed structures. It is worth highlighting that the monopile is laterally unconstrained, allowing full freedom across all its DOFs. For obtaining the eigenvalues of the crane barge, the monopile and the hook are assumed as fixed bodies. However, since the crane barge is connected to the hook and the monopile via lifting wire, it is not free, and this has effect on surge, sway, and yaw responses of the barge. The analysis for the coupled system is provided in Appendix A. The natural periods for the heave, pitch, and roll motions of the crane barge suggest that larger motions occur when the wave period (4–20 s) aligns closely with these natural periods. The crane barge can experience large, coupled heave and pitch motions when the wave period approaches 7.5 s. The same is valid for the coupled system.

Table 4
Eigen periods and eigen vectors of the crane barge rigid body motions.

Mode		1	2	3	4	5	6
Surge	[m]	−0.17	0.206	0.00	−0.001	**1.00**	−0.016
Sway	[m]	−0.001	0.001	0.108	−0.155	−0.016	**−0.938**
Heave	[m]	−0.13	**−0.617**	0.00	0.00	0.005	−0.001
Roll	[deg]	−0.007	0.005	**1.00**	−0.081	−0.002	−0.003
Pitch	[deg]	**1.00**	**−1.00**	0.003	−0.009	0.004	0.009
Yaw	[deg]	−0.022	0.013	−0.078	**−1.00**	−0.003	**1.00**
Natural period	[s]	5.282	7.562	14.205	53.331	131.82	1034.90

Table 5
Eigen periods and eigen vectors of laterally unconstrained monopile rigid body motions.

Mode		1	2	3	4	5	6
Surge	[m]	0.00	−0.509	0.495	0.145	0.147	0.00
Sway	[m]	0.00	−0.495	−0.509	0.147	−0.145	0.00
Heave	[m]	**−1.00**	0.00	0.001	0.00	−0.001	0.00
Roll	[deg]	0.005	**0.972**	**1.00**	**1.00**	**−0.985**	0.00
Pitch	[deg]	0.005	**−1.00**	**0.972**	**−0.985**	**−1.00**	0.00
Yaw	[deg]	0.005	0.00	0.00	0.00	0.002	**1.00**
Natural period	[s]	0.664	1.820	1.820	9.966	9.968	16.256

Table 6
Tension force in the lifting wire.

	Unit
Barge translational motion	[m]
Barge rotational motion	[deg]
Monopile lateral motion in x-dir.	[m]
Wire tension the X-component	[N]
Wire tension the Z-component	[N]

For the monopile, roll and pitch motions are sensitive to wave periods. The first mode is dominated by the heave motion of the monopile, with the heave stiffness primarily provided by the lifting wire's axial stiffness. Modes 2 through 5 involve a combination of rotational motion in the vertical plane. The final mode is characterized by pure yaw motion. The eigenvectors in Table 5 indicate that modes 2 and 3 are symmetric, sharing the same eigen-periods but occurring in different planes. The same symmetry and correspondence are observed for modes 4 and 5.

Interpreting the twelve eigenmodes of the coupled system is challenging due to the coupling effects. However, it is generally observed that the barge's motions slightly decrease the natural periods of the monopile's rotational modes. Additionally, the natural period of the barge's roll motion is reduced by the influence of the lifting system.

3. Model development

This section outlines the methodology for constructing the model for vibratory pile extraction. The condition of still water is considered in this section. The effects of incident waves will be examined separately in the subsequent section. The key simulation parameters which are going to be analyzed in this study are presented in Table 6. Global coordinate system is referred when mentioning to positions and directions.

3.1. Lifting without external loads

SIMA software offers the capability to conduct both static and dynamic analyses. Conducting a static analysis is a prerequisite for the dynamic analysis, as it assesses the equilibrium state of the system. SIMA offers two distinct algorithms for determining the equilibrium position of a system: the Newton-Raphson method and the transient method. The Newton-Raphson method is typically faster for systems involving a single body, as it relies on a linearized model of the system for its calculations. Conversely, the transient method is more robust, particularly

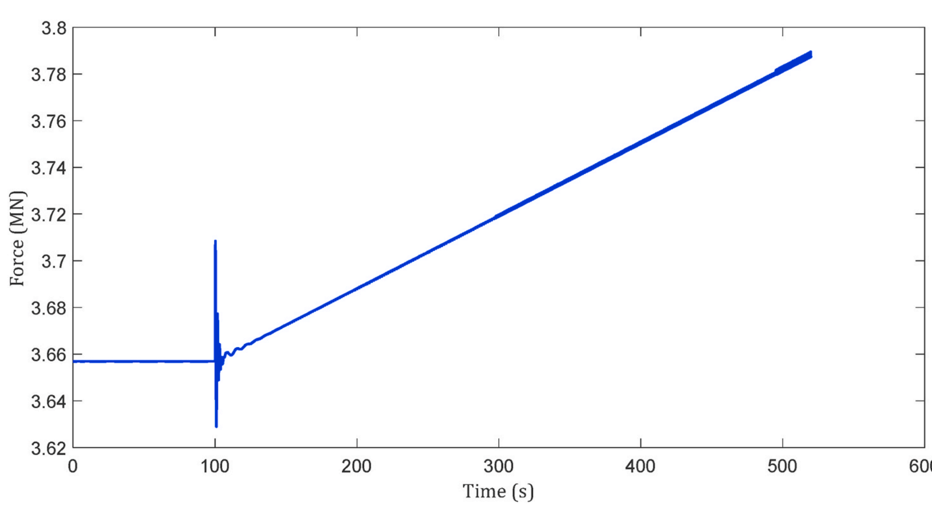

Fig. 5. Tension force in the lifting wire in z-dir.

Table 7
Tension force in the lifting wire.

	Unit	Value
Analytical	[MN]	3.761
Numerical	[MN]	3.789
Error	%	0.74

for systems with multiple bodies or significant non-linearities (e.g., fenders, dynamic positioning systems, etc.). Due to its versatility and reliability, the transient method is recommended as the default approach for equilibrium computations (SIMA Documentation) and has been chosen in the present study. During the static analysis, as the weight and buoyancy of the monopile are transferred to the lifting wire and subsequently to the crane barge, the coupled system achieves equilibrium. This equilibrium state results in a pitch angle of 1.686° in the crane barge. The monopile finds a new position that is attributed to the absence of any resistance or constraints acting on it.

SIMO provides two integration methods for time-domain analysis: the Runge-Kutta method and the modified Euler method (SIMA Documentation). A three-stage Runge-Kutta scheme is employed within each subdivision of the time increment. The primary objective of the simulation without exposure to external loads is to conduct a validation study to assess the accuracy of the model. As outlined in Section 2.3, the water depth is 30m and the monopile's lower tip is positioned 17 m below seabed level. Therefore, lifting to extent of 17m is necessary to extract the monopile from the seabed. Upon lifting the monopile to this level, it becomes buoyant with a submerged length equal to the water depth (30 m). At this moment, the tension force in the lifting wire should be equal to the total weight of the monopile, vibro-hammer and hook minus the buoyancy force acting on the submerged part of the monopile. Through straightforward hydrostatic calculations, the tension force in the lifting wire is determined to be 3.761 MN. Fig. 5 illustrates the time history of the tension force extracted from SIMA. The numerical value indicates a tension force of 3.789 MN when the monopile tip is out of the seabed. By comparing the numerical and analytical values (as presented in Table 7), it can be inferred that at the end of the lifting process, when the monopile is completely extracted from the seabed, the disparity between the results is minimal. The relative error is found to be approximately 0.74%, which is well within acceptable bounds for engineering simulations of this nature. This level of accuracy underscores the reliability of the model and its suitability for predicting the behavior of monopile vibratory extraction operations.

As depicted in Fig. 5, the winch motion starts at $t = 100$ s to mitigate transient effects on the motion of the monopile. Thus, the simulation time is 520 s, consisting of 100s delay in winch start and 420 s of extraction from seabed. At beginning of the lifting operation, a transient behavior is observable in the lifting wire.

Fig. 6 displays the translational and rotational responses of the crane barge. The responses of the crane barge are measured in its reference point, located at $(-53, 0, -3.6)$. Notably, the surge, heave, and pitch motions of the barge are most affected. At the onset of the lifting operation, the barge undergoes a brief period of partial transient oscillation. As the operation progresses, the pitch angle shifts from 1.686° to 1.746°, and the heave displacement increases from $-3.538\,m$ to $-3.546\,m$. These increases originate from the increase in the monopile's apparent weight in air. Additionally, during the lifting operation, the barge moves away from the monopile by a distance around 2 cm, because of the geometry of the lifting system. It is worth noting that the crane barge draft has changed from initial value of $-3.6\,m$ to $-3.538\,m$,

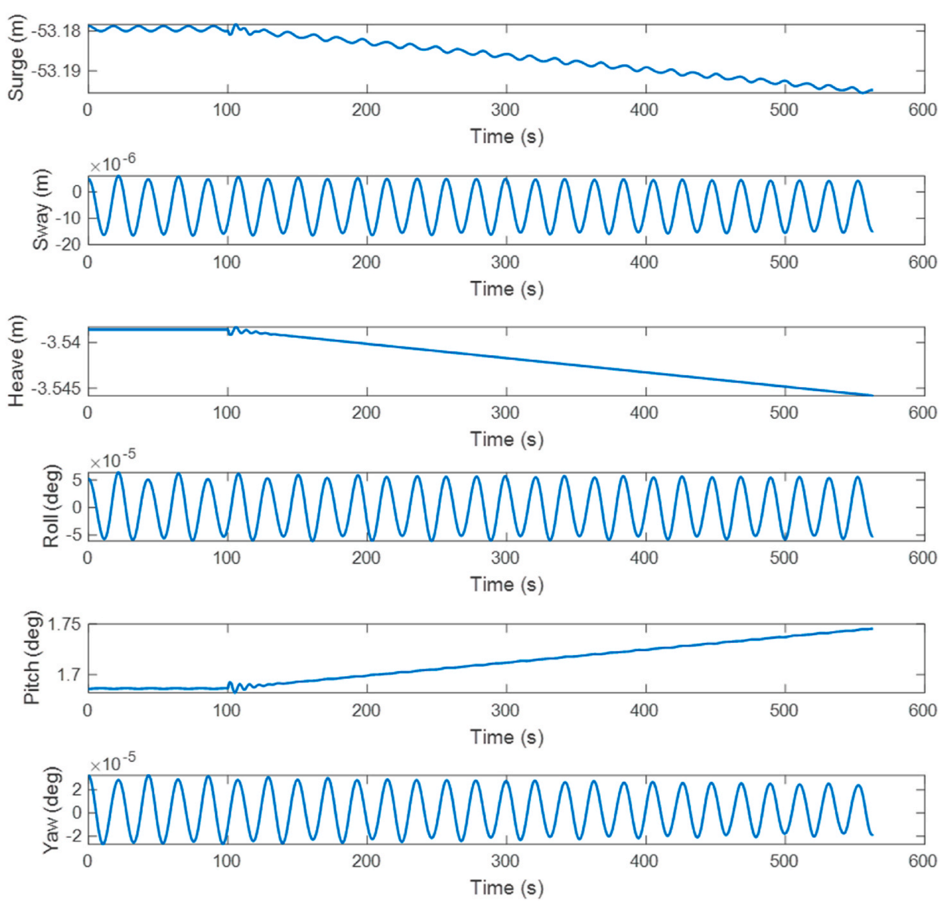

Fig. 6. Crane barge's response during lifting monopile.

Table 8
Eigen periods and eigen vectors of the constrained monopile.

Mode		1	2	3	4	5	6
Surge	[m]	**1.00**	**−1.00**	0.00	0.01	0.01	0.00
Sway	[m]	**1.00**	**1.00**	0.00	0.01	−0.01	0.00
Heave	[m]	0.00	0.00	**−1.00**	0.00	0.00	0.00
Roll	[deg]	−0.135	−0.135	0.005	**1.00**	**−1.00**	0.00
Pitch	[deg]	0.135	−0.135	0.005	**−1.00**	**−1.00**	0.00
Yaw	[deg]	0.00	0.00	0.005	0.00	0.00	**1.00**
Natural period	[s]	0.546	0.546	0.644	3.75	3.75	16.256

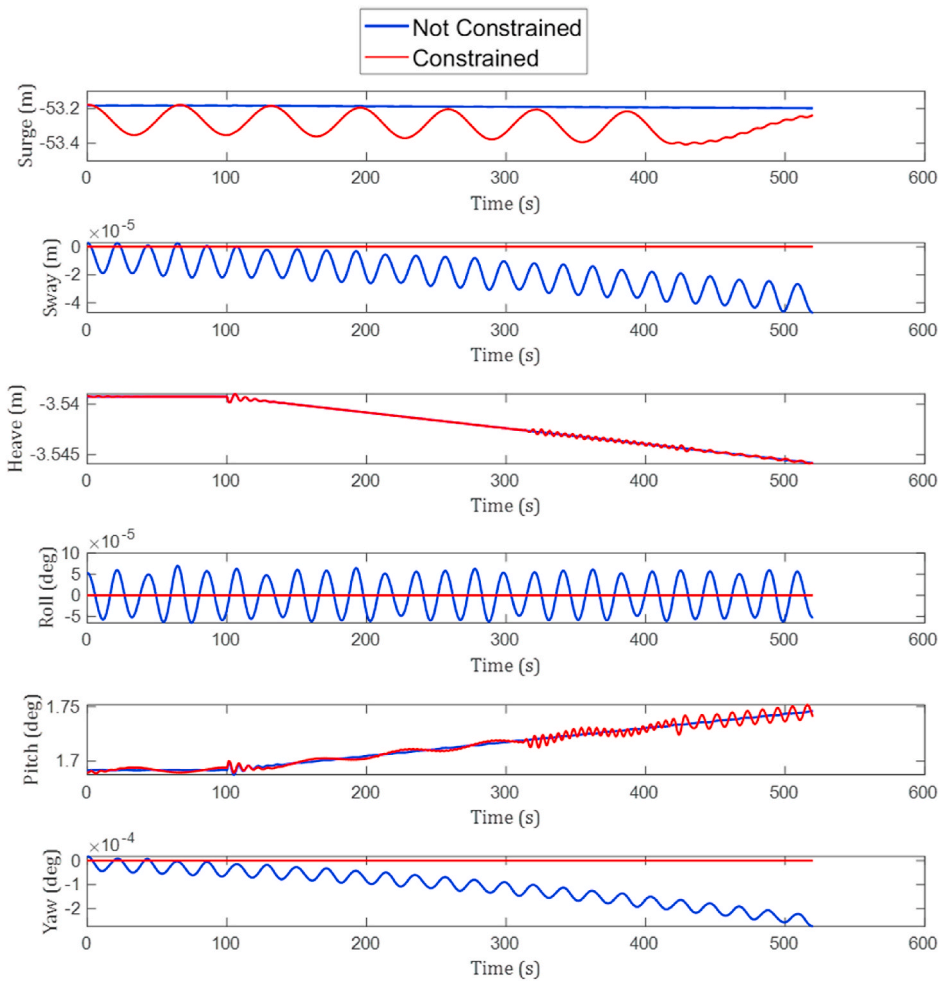

Fig. 7. Crane barge's response without and with constraints on the monopile.

which is due to the trim the barge has undergone after reaching to static equilibrium.

As previously discussed, the monopile was initially modeled without any constraints. This leads to a lateral displacement of 6 cm in the positive x-direction. This condition is unrealistic, as soil stiffness would typically restrict the monopile's lateral movement until it is fully released from the seabed. However, rotational displacements may occur as more of the buried length becomes unrestrained. Additionally, implementing constraints on the monopile is crucial for studying the extraction process in rough sea conditions. Without these constraints, both the monopile and the crane barge are susceptible to displacement by incoming waves. Therefore, it is necessary to introduce constraints on the monopile to achieve a more accurate simulation of vibratory monopile extraction.

Incorporating constraints on the monopile's movement can be achieved through various features available in SIMO, such as defining lateral stiffness, or adding components like docking cone, bumpers, and fenders. In this study, fenders are utilized to restrict the monopile's lateral movements. Fenders are commonly employed in offshore operations to prevent collisions and maintain a safe distance between floating bodies. Pneumatic rubber fenders provide a reaction force that increases progressively with compression. Introducing a fender into the system offers a compressive force parallel to the normal vector of the sliding plane, and frictional force along the sliding plane. However, in this case, the frictional force is set to zero by assigning static and dynamic friction coefficients of zero, as the soil's frictional force is accounted for separately via a DLL. Two sets of fenders are introduced to the system by defining fender points along external surface of the monopile and fender plane for each set on two fixed bodies close to the monopile.

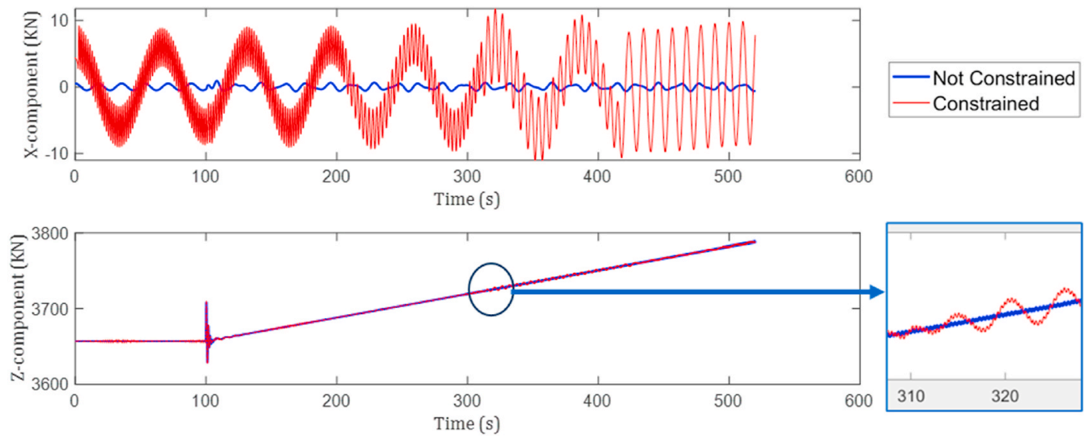

Fig. 8. Tension in the lifting wire.

To design a fender system for marine operations as an energy-absorbing device, it is essential to estimate the required energy absorption capacity. The PIANC guidelines (Hong et al., 2022) provide a methodology for estimating kinetic energy in such scenarios. However, the primary objective of incorporating a fender into the system in this study is to impose restrictions on the monopile's movement. To achieve this objective, a parametric study has been conducted. Within this study, a linear reaction force and a damping force are defined for a deformation of 100 mm, with magnitudes of 10 MN and 1 MN, respectively. These parameters are chosen to effectively constrain the monopile's lateral displacement, ensuring a more accurate representation of the system's behavior. Introducing constraints on the monopile changes its natural periods and modes. The eigen-value analysis results of the monopile are presented in Table 8.

The dynamic response of the crane barge with the fender constraint applied to the monopile is illustrated in Fig. 7 and can be compared to the previous scenario where no constraints are applied. The most notable impact of the monopile constraint is observed in the surge motion of the barge. Following the static phase, the crane barge is displaced away from the monopile as it floats freely. Subsequently, it begins to oscillate with a period of approximately 63.5 s, with the center of oscillation shifting away from the barge's initial position. Toward the end of the lifting process, the barge's behavior changes as it approaches its initial position. This change is attributed to the extraction of the monopile from the seabed, which effectively reduces the constrained length and stiffness within the system. The final position of the crane barge is 6 cm away from its initial position.

The application of constraints on the monopile also affects the horizontal component (x-direction) of the lifting wire tension, as illustrated in Fig. 8. Two distinct oscillatory force components are observed in the lifting wire tension. The lower-frequency component corresponds to the oscillatory motion of the crane barge, while the higher-frequency component is associated with the presence of the fender, which resists the inclinations of the monopile during the lifting process. Additionally, these oscillatory forces also influence the z-component of the wire tension, demonstrating the interconnected effects of the constraints on the system's dynamics. It is worth mentioning that y-component of the wire tension has been unaffected and zero whole throughout the lifting process. It is worth highlighting that for the rest of this study, constraints on the monopile are preserved.

3.2. *Effect of vibro-hammer centrifugal force*

In this step, the centrifugal force generated by the vibro-hammer is applied to the monopile. During the reference vibratory extraction process, the vibro-hammer operated at a vibration frequency of 19.5 *Hz*

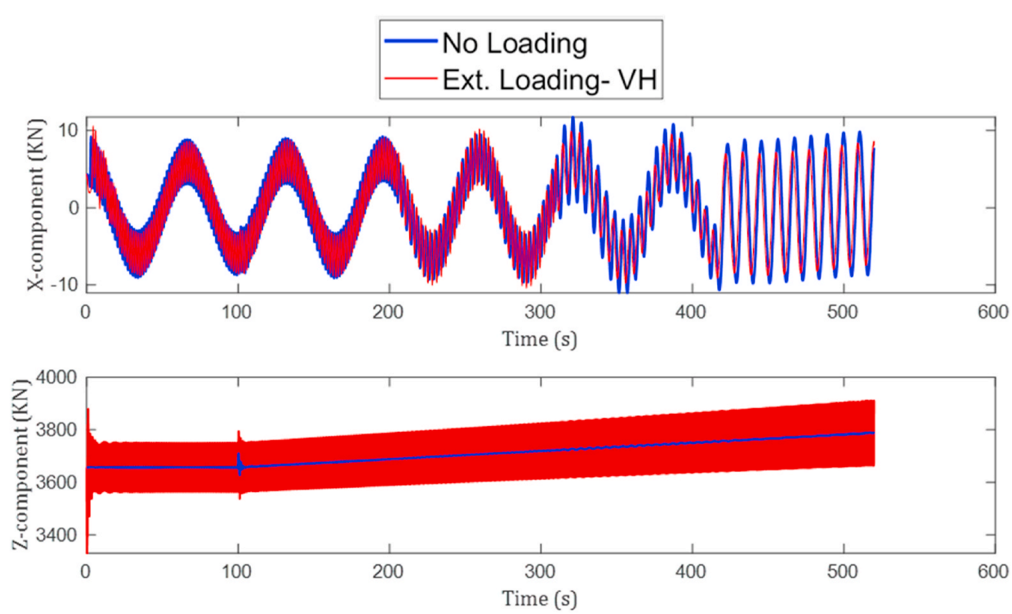

Fig. 9. Tension force in the lifting wire in z-dir. during vibro-hammer operation.

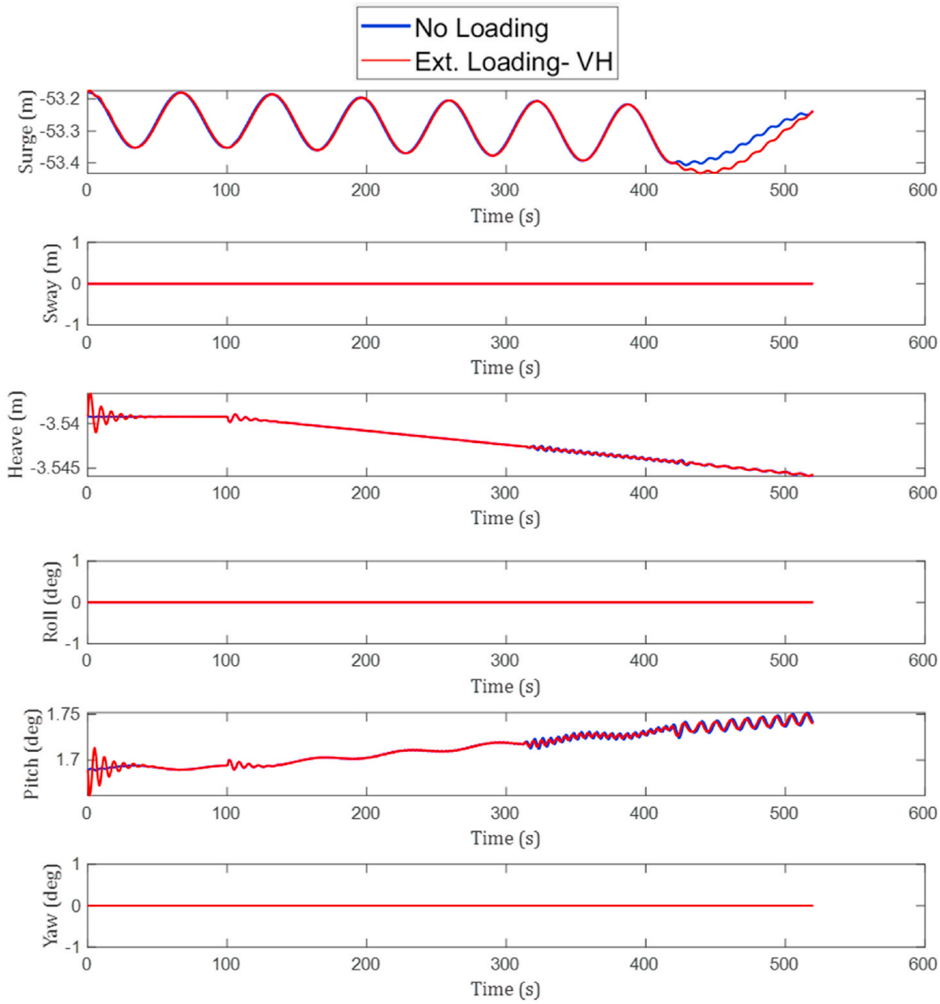

Fig. 10. Effect of vibro-hammer on barge's response while it is operating.

(Salahshour et al., 2023; van Dorp et al., 2021), generating a centrifugal force of 9.607 *MN*. This force is input into the SIMO multi-body code using an external DLL, which is provided by a Python subroutine. SIMO offers the capability to define external loads in various forms, including constant, harmonic, and ramp-loading configurations. However, the module has certain limitations when specifying loads based on custom-defined functions or importing data directly from external spreadsheets. To address these constraints, the DLL functionality enables the integration of soil resistance data derived from the results of external analyses. Additionally, the centrifugal force generated by the vibro-hammer is modeled as a sinusoidal function within a Python script. This approach facilitates the precise application of the force at a user-defined time, enhancing the flexibility and accuracy of load specification. The effect of vibro-hammer centrifugal force on the lifting wire tension is illustrated in Fig. 9. As it can be seen, the centrifugal force induces an oscillatory force in the lifting wire, with an amplitude of approximately 0.1 *MN*. Two fluctuations are observed: one at the onset of the process and the other at the initiation of the lift after 100 s. The former originates from activation of the vibro-hammer, and the latter is caused by start of winch winding. However, the maximum amplitude of these fluctuations increased from 3.8 *MN* to 3.9 *MN*, indicating 2.6% rise.

The effect of the high cyclic centrifugal force of the vibro-hammer on the crane barge's dynamic response is shown in Fig. 10. Response of the barge while exposed to the vibro-hammer load is shown with legend of "Ext. Loading- VH". Compared to the previous case, only minor effects on the barge's response are observed. This observation suggests that despite the significant magnitude of the centrifugal force, the transmitted load to the barge remains relatively low. The rapid change in the direction of the applied force mitigates its effect on the barge. Consequently, the use of vibro-hammers presents a distinct advantage due to their reduced impact on the barge's overall dynamic response. Monopile's dynamic response is unchanged with respect to the previous case. It is worth highlighting again that simulations for developing the model are conducted for 520 s, consisting of 7 min of extraction plus 100 s delay for prevention of transient behavior in the system.

3.3. *Effect of soil resistance*

In this step, only soil resistance is applied to the monopile. The pile-soil interaction was analyzed in a separate study that investigated the effects of high cyclic loading to extract a monopile from saturated sandy seabed using ABAQUS finite element software (Salahshour et al., 2023). The numerical results indicated a significant reduction in soil resistance, which decreased to 22% of its initial value. This reduction means there is a demand to lower crane uplift force, allowing for the use of a smaller floater with reduced lifting capability. It is important to note that the soil in this study has been modeled as a homogeneous material (Salahshour et al., 2023), whereas in reality, varying soil types may be encountered along the depth. Such variations can lead to non-uniform soil resistance, as different soil layers may exhibit distinct degradation behaviors or susceptibility to liquefaction under cyclic loading. This variability could result in non-uniform reductions in soil resistance throughout the extraction process. Nevertheless, in the present study, the effects of soil

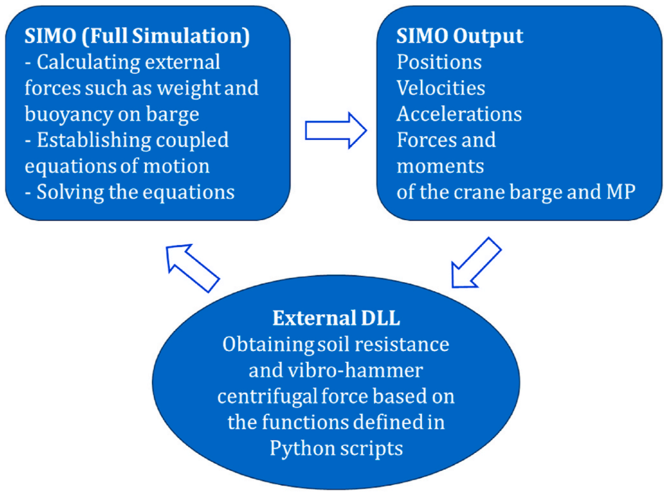

Fig. 11. Implementation of DLL in SIMO.

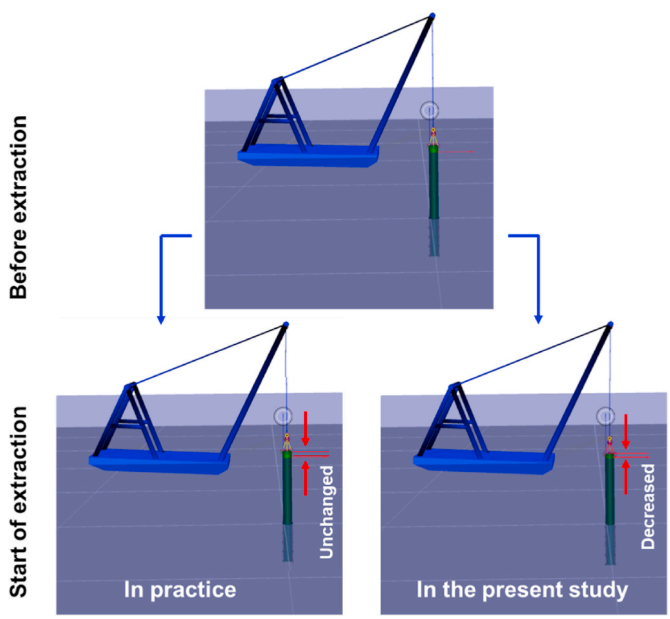

Fig. 12. Change of the pitch angle before lifting and in the beginning of the extraction.

degradation due to cyclic loading are incorporated using a linear function, where the soil resistance is progressively reduced to zero by the end of the extraction process.

The soil resistance is applied to the monopile via a DLL. A schematic of DLL implementation is shown in Fig. 11. The soil resistance while exposed to cyclic loading of the vibro-hammer starts from 1.7 *MN* and gradually approaches to zero at the end of the extraction. As previously mentioned, the extraction process begins after 100 s to mitigate transient behavior in the system. Basically, the soil resistance is at its maximum magnitude at the start of the process.

It is worth highlighting that without using the vibro-hammer to reduce soil resistance, extracting the considered monopile with the modeled crane barge is impossible since the soil resistance of 7.5 MN to pullout the monopile results in submergence of barge's deck.

In the numerical simulation, applying soil resistance to the monopile induces a downward motion, which is demonstrated in Fig. 12. This happens because no constraint is applied to the monopile to prevent its vertical movement. This increases the crane barge's pitch motion. In practice, the monopile does not experience downward motion. However, an increase in the floater's pitch motion is expected when crane uplift force is applied. This occurs because applying the crane load to the monopile via the lifting wire causes the floater to experience pitch due to the additional load on the lifting system. As the monopile is further extracted from the seabed and the soil resistance decreases due to the reduction in the contact surface of the monopile-soil interface, the pitch angle of the floater decreases. In the beginning of the extraction process, the pitch angle of the crane barge increases from 1.686° to 3°, and then gradually decreases to a final value of 1.74°, as the monopile is extracted and soil resistance diminishes. This final value of pitch is in agreement with the final pitch angle presented in Section 3.1, i.e., 1.746°.

Fig. 13 presents the motions of the crane barge in different DOFs when the monopile is exposed to only soil resistance. The surge motion of the crane barge is initiated when the winch begins winding. At this point, the crane barge moves away from the monopile by approximately 1.4 m before entering an oscillatory motion as it seeks to reach equilibrium. However, during the final 100 s of the extraction process, the period of the oscillatory motion changes. This change is likely attributed to the reduction in the embedded length of the monopile, as the embedded length directly influences the system's stiffness. Moreover, the heave motion of the barge initially changes from $-3.538\,m$ to $-3.677\,m$ at the beginning of the lifting operation. It then approaches the final value of $-3.546\,m$, similar to the scenario with no external loading. Other motions of the crane barge, including sway, roll, and yaw, are negligible.

Fig. 14 presents tension in the lifting wire. The x-component of the wire tension exhibits a significant peak at the onset of the lifting process, exceeding the values observed in the two previous scenarios—specifically, without external load and with the application of vibro-hammer force—by more than tenfold. This tension component closely follows the harmonic motion of the crane barge. However, during the final 100 s of the process, it is predominantly influenced by the displacement of the monopile. As the monopile is progressively released, it undergoes a swinging motion, which significantly impacts the wire tension in the x-direction.

Initially, the z-component of wire tension is 3.645 *MN*, exhibiting some transient oscillations at the beginning of the simulation. When the extraction process starts, the lifting wire tension increases to around 6.02 *MN*, rather than the expected 5.345 *MN*, which is the sum of the monopile's submerged weight and soil resistance. The additional tension in the lifting wire is initially caused by the start of the winch winding process, resulting in a sudden snapping load. However, this load dissipates (after around 30 s) as the lifting operation continues.

3.4. Vibratory extraction

In this section, both the vibratory hammer's centrifugal force and soil resistance are applied to the monopile during lifting, resembling the real vibratory monopile extraction operation in calm water without incoming waves. The dynamic response of the crane barge is presented in Fig. 15.

The response of the crane barge closely mirrors the behavior analyzed in Section 3.3 where only soil resistance is applied to the monopile. This underscores that the coupled system response is predominantly influenced by the soil resistance, despite the vibro-hammer exerting a substantial force of 9.607 *MN*. The high frequency and rapid directional changes of this force mitigate its overall effect on the system.

Fig. 16 shows the tension force in the lifting wire during vibratory monopile extraction. This tension includes an oscillatory component, originating from the vibro-hammer's centrifugal force, in addition to the baseline tension in association with soil resistance. However, the maximum tension in the lifting wire that happens at the beginning of the extraction increases to 6.1 MN (compared to condition described in section 3.3). This increase originates from the vibro-hammer centrifugal force. The oscillatory component starts with an amplitude of

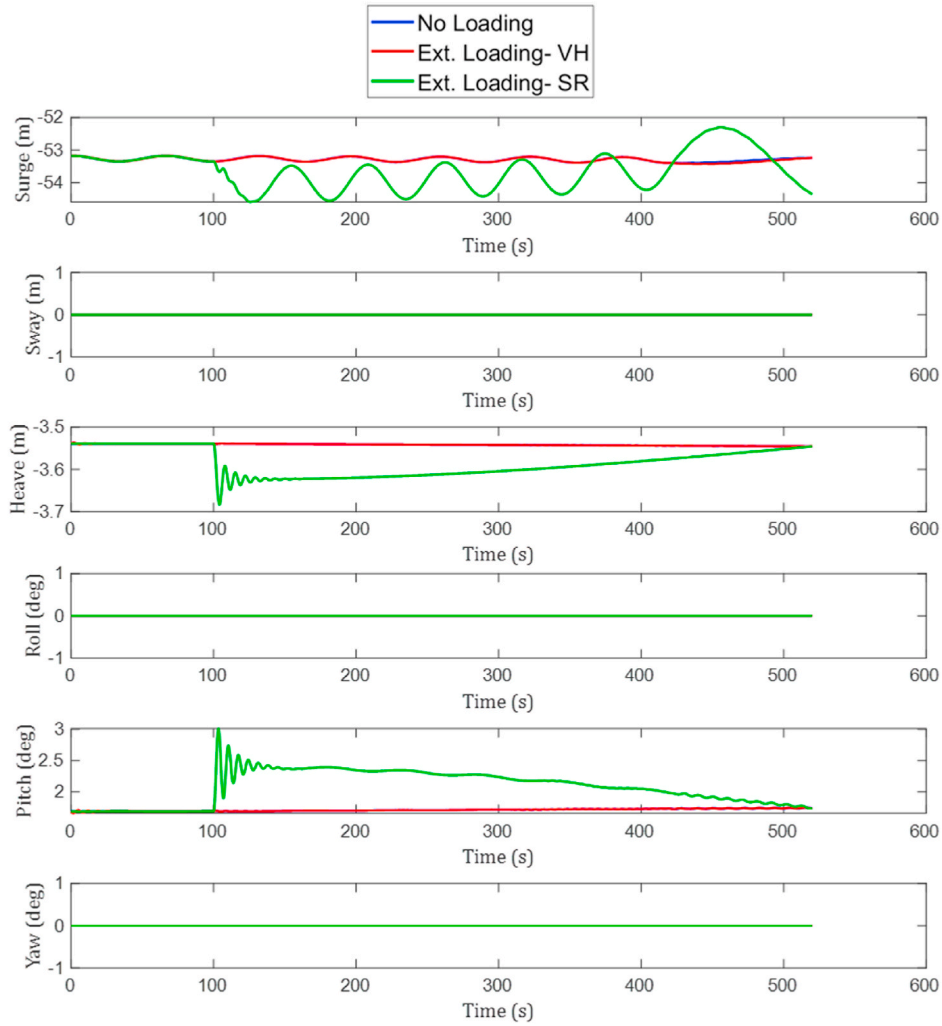

Fig. 13. Crane barge's response while soil resistance is inserted to the monopile.

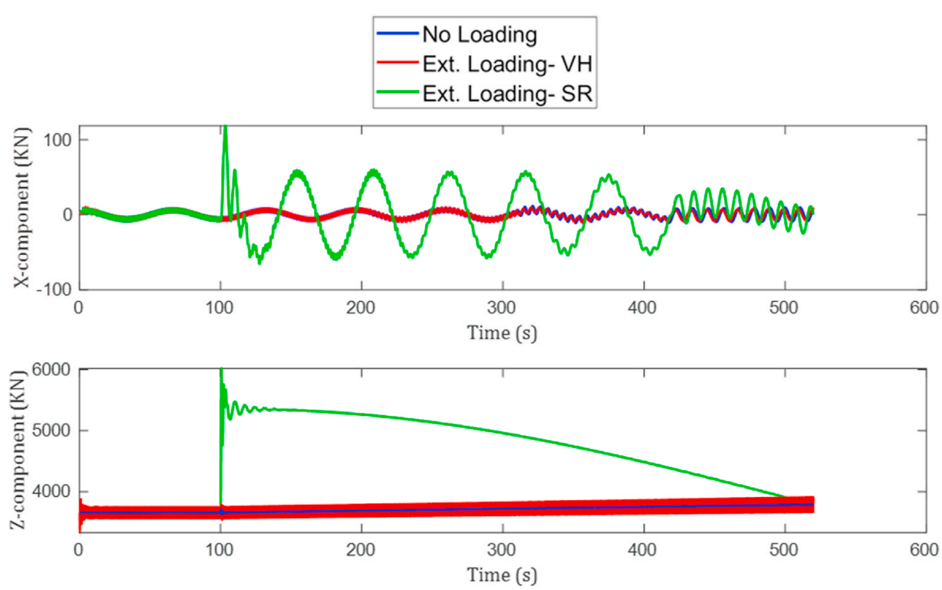

Fig. 14. Lifting wire tension under effect of soil resistance.

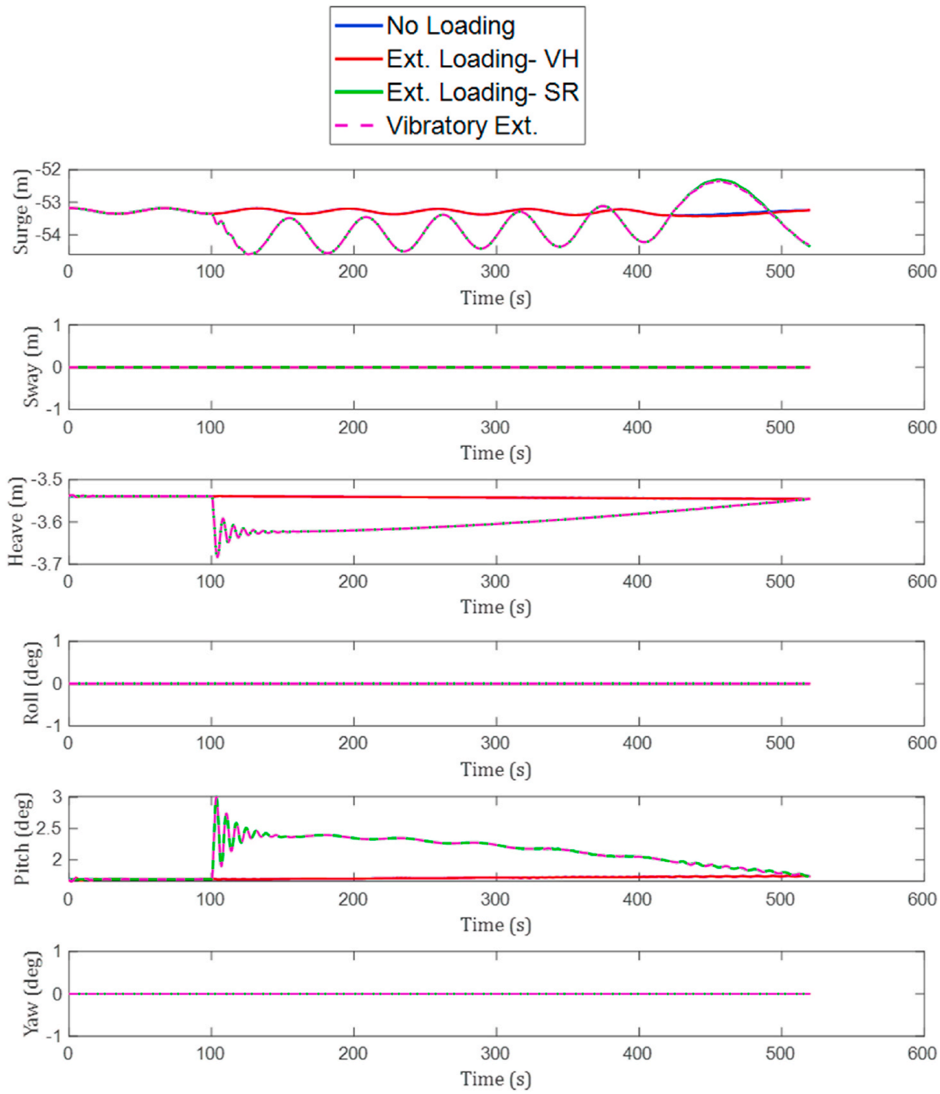

Fig. 15. Crane barge's response during vibratory extraction.

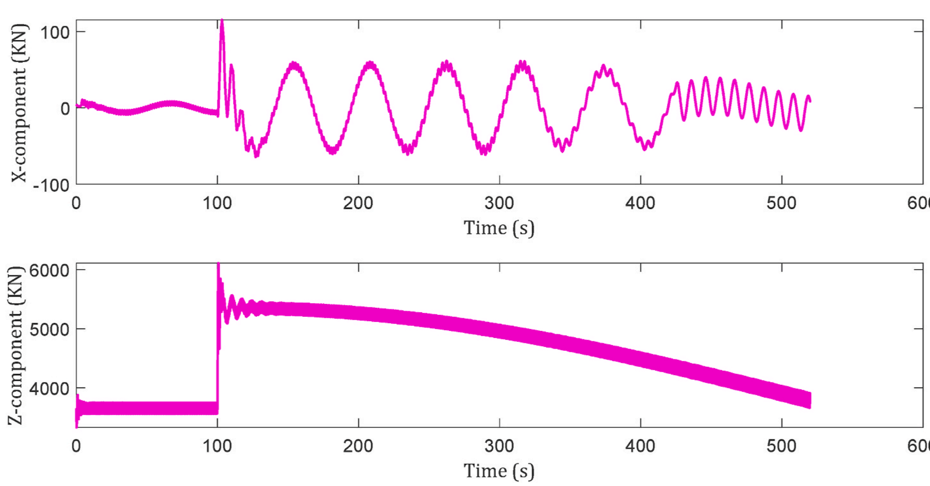

Fig. 16. Lifting wire tension during vibratory extraction of the monopile.

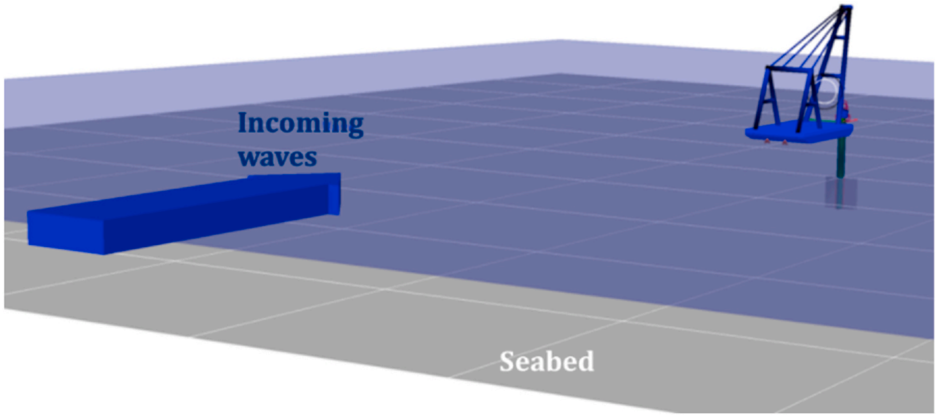

Fig. 17. Dynamic positioning control system using four thrusters.

Table 9
Sea conditions with long-crested waves.

Sea State	H_s (m)	T_p (s)
SS1	1	5
SS2	1	11

approximately 0.09 *MN*, gradually increasing to 0.11 *MN* by the end of the extraction. This increase in amplitude is attributed to the monopile's apparent weight increase as it is extracted from the seabed and more part of it leaves water.

4. Dynamic responses under operational sea conditions

In this section, the vibratory extraction of the monopile is analyzed under operational sea conditions for two distinct sea states characterized by long-crested waves. The incoming wave direction is considered zero degree as DNV recommendation practice requires a head sea positioning for marine lift operations with an offset of $\pm 15^\circ$ (DNV). The orientation of the crane barge is shown in Fig. 17. The first part of the analysis focuses on the key dynamic responses of the crane barge, including surge, heave, pitch, and the tension in the lifting wire. In the second part, the application of dynamic positioning (DP) to the crane barge is examined to assess its effect on these parameters. The effects of current and wind loads are not considered.

4.1. Responses in waves

The JONSWAP wave spectrum is used to simulate both the long-crested irregular waves, which can be expressed as (DNV GL-CG-0130, 2018):

$$S_J(\omega) = \frac{\alpha g^2}{\omega^5}\left(-1.25\frac{\omega_p^4}{\omega^4}\right)\gamma^{\exp\left(-\frac{(\omega-\omega_p)^2}{2\beta^2\omega_p^2}\right)} \tag{5}$$

The spectrum parameter β is equal to 0.07 when $\omega \le \omega_p$, and 0.09 when $\omega > \omega_p$. α is defined as:

$$\alpha = 5.061 H_s^2 T_p^{-4}[1 - 0.287 \ln(\gamma)] \tag{6}$$

where, H_s is the significant wave height, and ω_p and T_p correspond to the peak angular frequency and the peak period, respectively. γ is the peak enhancement factor. The considered sea conditions of this study are presented in Table 9.

Wave time series are generated by discretizing the JONAWAP spectrum into a finite number of harmonic components with uniformly

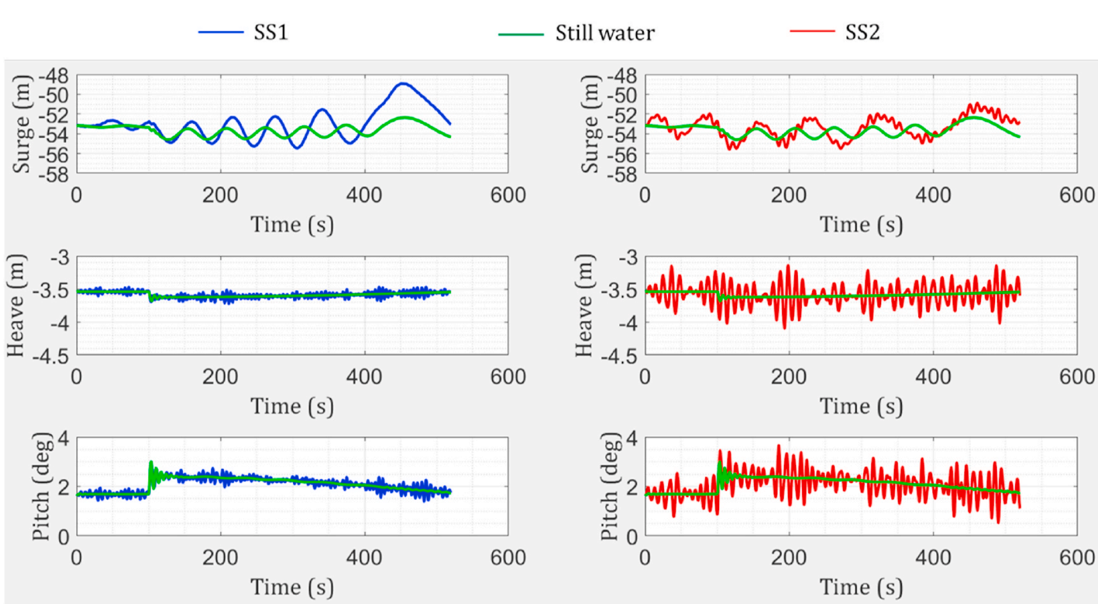

Fig. 18. Dynamic response of the crane barge in short crested and long crested waves.

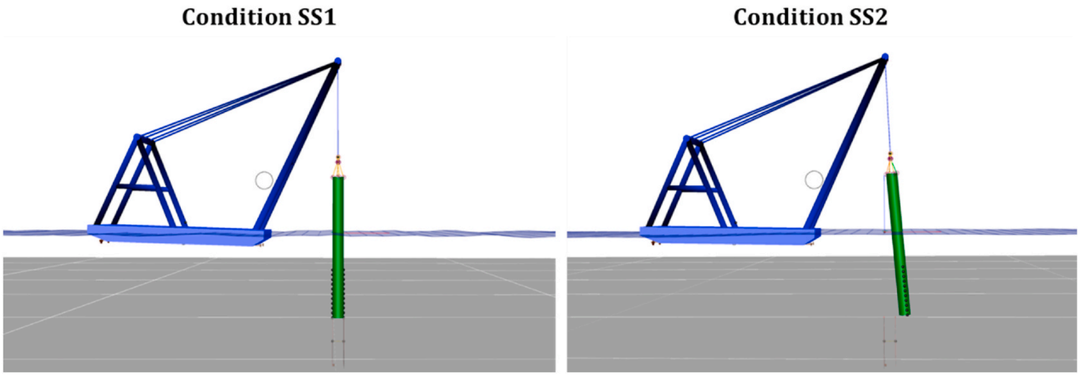

Fig. 19. Monopile position at end of extraction.

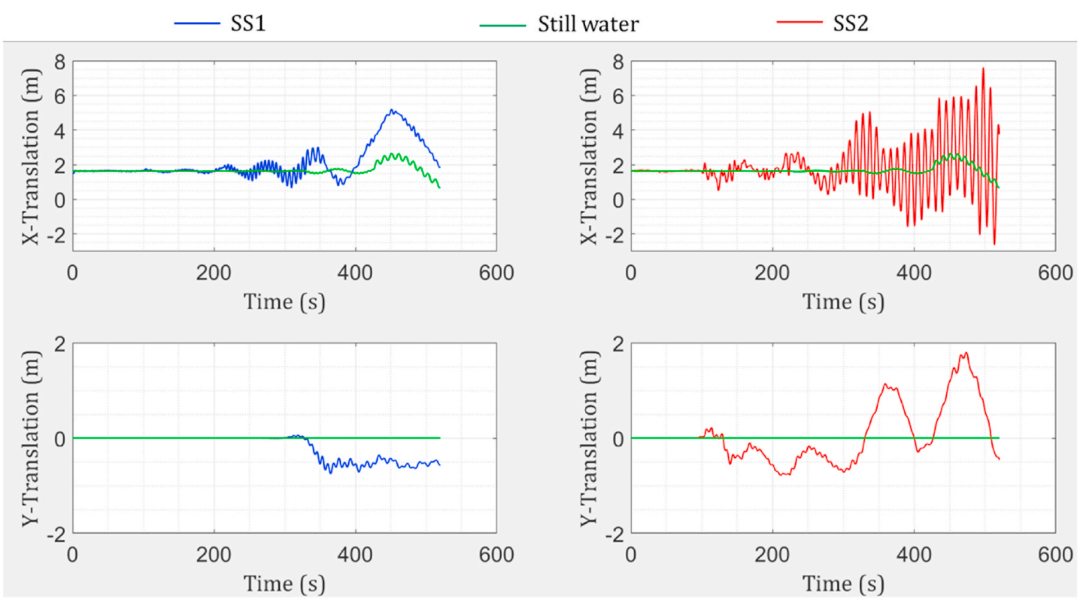

Fig. 20. Monopile motion in X- and Y-directions.

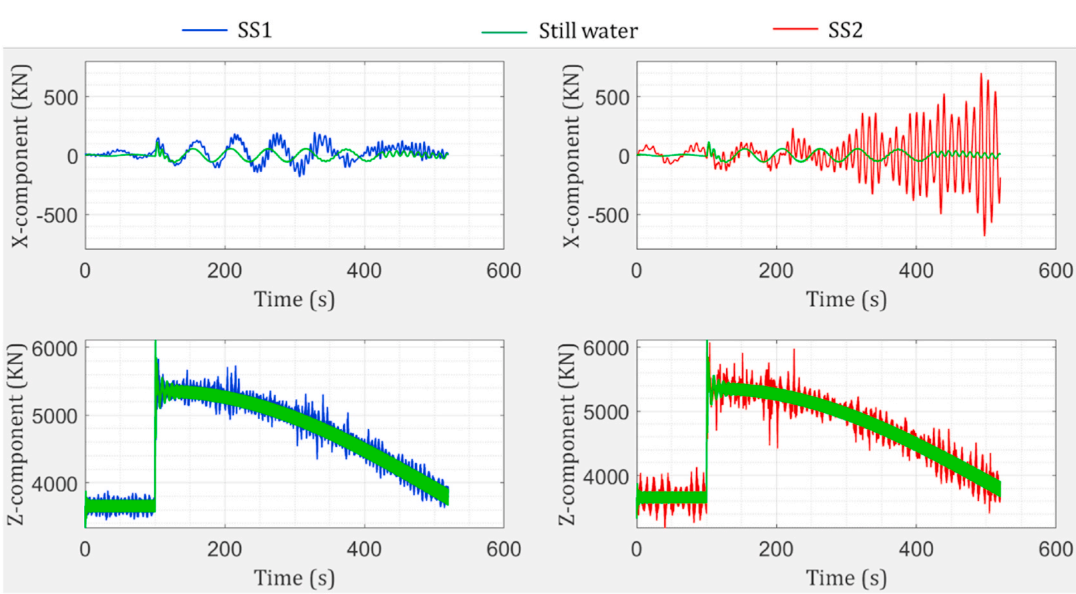

Fig. 21. Components of tension force in the lifting wire.

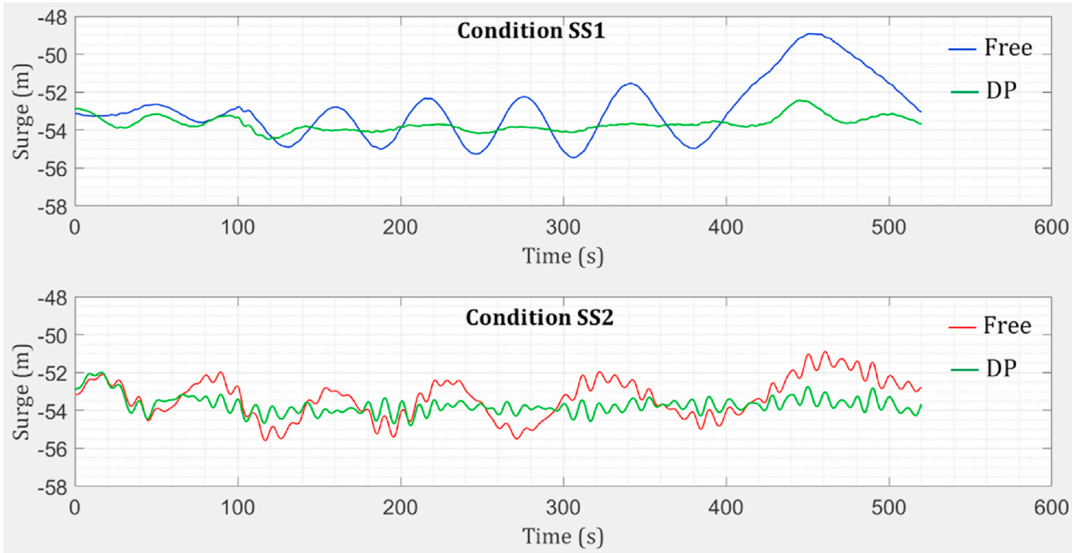

Fig. 22. Surge response of the crane barge in two sea states under DP control.

distributed phase angles, utilizing the Fast Fourier Transform (FFT). The phase angles are determined using a pseudo-random number generator, with the seed specified by the user (Sima Documentation). Altering the seed value produces a different realization of the time series, which subsequently leads to variations in simulation results when wave loads are included. To capture the randomness of sea states effectively, 20 realizations are generated for each simulation, each corresponding to a unique seed. During the removal of the monopiles, the orientation of the crane barge is adjusted so that the head sea condition is achieved. The configuration of the lifting system ensures that if the thruster system fails, the crane barge will not collide with the monopile.

Fig. 18 presents the dynamic response of the crane barge when exposed to long-crested waves. For comparison, the response under still water conditions is also shown in green. It can be observed that the surge response of the crane barge is affected more in the case of long-crested waves with smaller T_p, i.e., SS1, while the coupled responses of the crane barge for heave and pitch motions are more pronounced in long-crested waves with larger T_p, i.e., SS2. For condition SS1, the harmonic displacement of the surge motion is larger compared to SS2, and at the last 100 s of the vibratory extraction, the barge drifts towards the monopile. However, it moves back to a position very close to beginning of the operation because of restoring force applied to it by the monopile. Under condition SS2, the heave motion exhibits a large amplitude, reaching approximately 40 cm. This significant vertical displacement results in the monopile being released from the seabed earlier than anticipated. While the expected release time was 7 min, the monopile detaches after 6.5 min of vibratory extraction. This corresponds to a simulation time of $t = 490\,s$, considering the extraction process commences at $t = 100\,s$.

The monopile positions under conditions SS1 and SS2 are presented in Fig. 19. For condition SS2, the detachment of the monopile from the seabed has a minimal impact on the barge's dynamic response. However, during the final 30 s of the simulation, the monopile swings freely. Due to the geometry of the lifting system, a safe distance is maintained between the monopile and the barge hull, preventing the development of critical conditions during this phase. Nevertheless, the subsequent stages of lifting the monopile out of the water could pose significant risks. Fig. 20 illustrates the monopile's movements in both the X- and Y-directions.

Fig. 20 demonstrates that significant movements occur in the monopile in both the X- and Y-directions under both conditions, with more pronounced motions observed in condition SS2. As the bottom portion of the monopile remains embedded in the seabed while the top is connected to the slings, the initiation of vibratory extraction induces oscillatory swinging. The amplitude of these oscillations increases as a greater portion of the monopile is extracted from the seabed. In condition SS2, a resonance phenomenon is evident, where the oscillatory motion amplitudes grow significantly. It is worth mentioning that the measurement point for monopile displacement is at distance of 3 m from its top head. This behavior can be attributed to the wave peak period ($T_p = 11\,s$) aligning closely with the monopile's natural periods in roll and pitch motions ($T_p = 9.974\,s$). For condition SS1, the monopile's movement in the X-direction closely follows the crane barge's surge motion, particularly as more of the monopile is freed from the seabed. No detachment of monopile from the seabed is observed in SS1.

In rough sea conditions, the increased motion of the crane barge leads to higher tension in the lifting wire, as illustrated in Fig. 21. The tension components in both the x- and z-directions are presented. The larger surge motion of the monopile under the condition SS2 results in a higher x-component of wire tension compared to the condition SS1. The maximum x-component of wire tension for SS1 is 197 KN, which is 71% increase compared to still water condition. The corresponding value for SS2 is 700 KN, which is more than 6 times increase. The x-component of the wire tension exhibits cyclic oscillations under SS2 condition, with magnitude varying between positive and negative values. This oscillatory behavior is driven by the monopile's swinging motion, where increased extraction from seabed alters the monopile's boundary conditions, resulting in creation of a pivot point. As the extent of monopile extraction increases, the amplitude of the swinging motion correspondingly intensifies, resembling the dynamics of an inverted pendulum. As shown in Appendix A, the monopile's roll motion will experiences resonance at its natural period of 11.5 s. This period is close to the SS2 peak period, potentially explaining the elevated tension magnitudes observed under this condition.

The peak values of wire tension in z-direction for both conditions of SS1 and SS2 are unchanged compared to the still water condition (overlapped in the graphs). While it is anticipated that the increased pitch and heave motions of the barge in rough sea conditions will also elevate the z-component of the wire tension, the lack of constraints on the vertical movement of the monopile shows small difference compared to the still water conditions. This observation indicates that further research is needed to more accurately predict the wire tension forces under varying conditions.

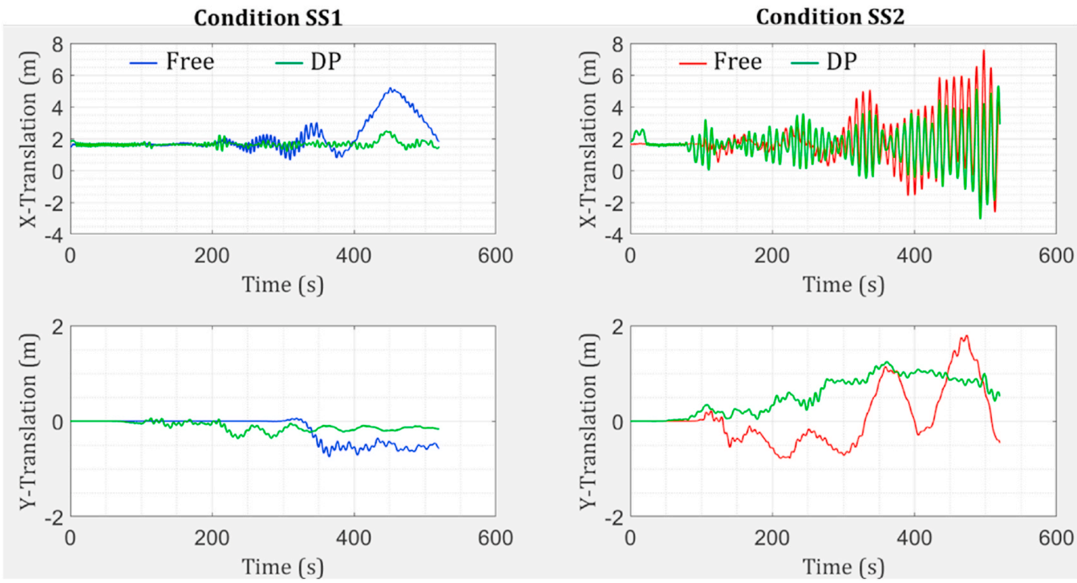

Fig. 23. Monopile motion in X- and Y-directions under active DP.

4.2. Dynamic positioning

According to the American Petroleum Institute (API), Dynamic Positioning (DP) is defined as a technique of automatically maintaining the position of a floating vessel within a specified tolerance by controlling onboard thrusters which generate thrust vectors to counter the wind, wave and current forces. The Kalman filter is a widely used algorithm in DP systems, developed based on modern control theory. It addresses some disadvantages of PID controllers, such as slow integral action and phase lag in control loops. The primary functions of the Kalman filter include (Cadet, 2003).

- Estimating vessel motion,
- Measuring vessel response,
- Determining the error between predictions and measurements,
- Determining the corrective action to be applied,
- Calculating and allocating appropriate commands to thrusters to achieve the desired corrective action.

The vessel model consists of equations of motion used to predict vessel movements under known forces and moments. To distinguish the wave-induced oscillatory part of the motion from other components, the total vessel motion is modeled as the sum of a low-frequency model (LF-model) and a high-frequency model (HF-model) (Cadet, 2003). The HF-model represents oscillatory wave components in vessel motion, while the LF-model represents motions induced by wind, thrust, and current in surge, sway, and yaw. This terminology has evolved, and these are now referred to as wave-frequency and low-frequency states (Fossen and Perez, 2009). The Kalman filter estimates both states, with wave-filtering achieved by using only the low-frequency states as feedback signals in the motion controller. The Kalman filter reduces measurement noise while providing estimates of velocities and rates when these are not directly measured.

As described in Section 2.2, the modeled crane barge is equipped with both bow and aft thrusters, which enables it to control surge, sway, and yaw motions. Nevertheless, only surge motion of the crane barge is of importance here since the other two responses are negligible. Each of these thruster systems is assumed to drive two propellers, as illustrated in Fig. 17.

In the DP system under consideration, each propeller is allocated a

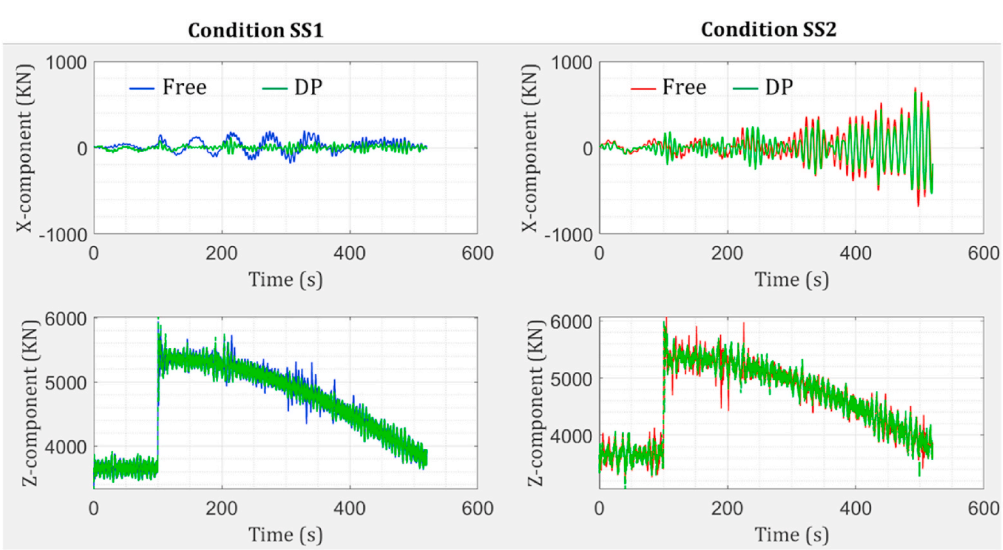

Fig. 24. Components of tension force in the lifting wire under DP control.

Fig. 25. Increase in pitch angle during vibratory extraction operation (Dieseko Group, 2017).

thrust force of 100 *KN*. The resulting surge motion for each sea state is shown in Fig. 22 and can be compared with the previous scenario without DP (referred to as "free"). As it can be observed, the DP system influences on the LF response of the crane barge. For both sea states, the DP system effectively reduces the amplitude of the surge motion, resulting in a more stable movement. In condition SS1, the DP system maintains the crane barge at a mean position of $x = -53.68\ m$, which represents a displacement of $0.5\ m$ from its initial position ($x = -53.18\ m$). Similarly, in condition SS2, the mean position of the crane barge is $x = -53.72\ m$, corresponding to a displacement of $0.54\ m$ from its initial position.

Fig. 23 presents the monopile displacements under conditions where the DP system of the crane barge is active. The results indicate a significant reduction in monopile movements in both the X- and Y-directions for condition SS1, suggesting that controlling the surge motion of the crane barge positively influences the horizontal components of the wire tension. However, this effect is less evident for condition SS2. For SS2, the horizontal component of the wire tension appears to primarily originate from the resonant motion of the monopile. While the DP system provides a partial reduction in monopile displacement compared to the scenario where the barge operates with an inactive DP system, the resonance effect in SS2 limits the overall effectiveness of the DP system in mitigating monopile movements.

The effect of the DP system on the lifting wire tension is depicted in Fig. 24. It is evident that application of the DP does not influence the z-component of the lifting wire tension. The activation of the dynamic positioning (DP) system has proven effective in reducing the horizontal component of wire tension for condition SS1. However, for condition SS2, the DP system has shown limited effectiveness. This discrepancy is attributed to the monopile's pronounced movements in the X-direction, which remain largely unaffected by the station-keeping capability of the barge. In SS2, the monopile's motions are significantly influenced by the passing waves, which dominate the system's dynamic response and limit the impact of the DP system.

5. Conclusion

Decommissioning of offshore wind farms involves several stages, with the removal of foundations being among the most challenging. Utilizing vibro-hammers for the complete removal of monopile foundations – the most widely used foundation type for bottom-fixed offshore wind turbines – can expedite the decommissioning process, reducing both time and costs. This study focuses on vibratory monopile extraction from a sandy seabed using a crane barge. The primary objective has been to analyze the dynamic response of the crane barge, monopile movements and the tension forces in the lifting wire.

A numerical model has been developed to separately examine the effects of vibro-hammer centrifugal forces and soil resistance on the monopile, followed by their combined application to simulate the real scenario of vibratory extraction. The results reveal that soil resistance is a key factor influencing the dynamic response of the crane barge. In addition to still water conditions, the response of the crane barge is investigated in two sea states comprised of long-crested waves, both with a significant wave height of $H_s = 1m$ but different peak periods, $T_p = 5s$ and $T_p = 11s$. The results indicate that larger peak wave period amplifies the heave and pitch motions of the crane barge, whereas shorter peak period have a more pronounced effect on its surge motion. Notably, the amplitude of the monopile's movements in the X- and Y-directions is significantly larger at a peak period of 11 s. This behavior is attributed to the proximity of the wave period to the monopile's natural period of roll and pitch motions, leading to resonant amplification of its movements.

The study also examines the response of the crane barge equipped with a dynamic positioning (DP) system controlled by a Kalman filter. The DP system effectively stabilizes the barge's position, significantly reducing surge motion during the operation. In sea conditions with a shorter wave peak period, the DP system successfully mitigates the horizontal movements of both the barge and the monopile in the X-direction, thereby reducing the horizontal component of tension in the lifting wire. However, in sea conditions with a longer peak period, although the DP system reduces the amplitude of the barge's surge motion, it does not significantly decrease the monopile's lateral movements or the horizontal component of wire tension. This is attributed to the monopile's response being influenced by the wave peak period, which is close to the monopile's natural frequency for roll and pitch motions, resulting in resonance.

CRediT authorship contribution statement

Soheil Salahshour: Writing – review & editing, Writing – original draft, Visualization, Validation, Software, Methodology, Investigation, Formal analysis. **Zhiyu Jiang:** Writing – review & editing, Supervision, Software, Methodology, Investigation, Formal analysis, Conceptualization. **Muk Chen Ong:** Writing – review & editing, Supervision, Resources, Project administration, Methodology, Funding acquisition, Formal analysis, Conceptualization. **Bjørn Skaare:** Writing – review & editing, Supervision, Methodology, Investigation, Formal analysis, Conceptualization.

Recommendations for future work

The complexity of the multi-body system necessitates comprehensive time-domain simulations and statistical analyses to achieve reliable results, particularly in assessing the operational safety of vibratory monopile extraction. As demonstrated in the numerical results and observed in real-world operations (see Fig. 25), the crane barge undergoes significant pitch and heave motions, particularly during the initial phase of the extraction process. Statistical analyses aimed at predicting extreme responses and establishing preliminary allowable sea states to guide monopile extraction operations using a crane barge remain topics for further investigation and will be addressed in future research.

Vibratory monopile extraction can be conducted using either a crane barge or a heavy lift vessel (HLV). In the case of the crane barge, lifting occurs from the stern, whereas for the HLV, lifting is performed from either the port or starboard side. A detailed operability analysis, including clarification of operational limit criteria and the estimation of suitable weather windows for vibratory monopile extraction using these vessels, is another potential area of study. Additionally, for safety considerations, the impact of ballast adjustments on the stability of the vessels and direction of incident waves could be analyzed.

As noted in this paper, no constraints were applied to the vertical movement of the monopile during the extraction process. In practice, however, soil imposes constraints on the monopile's vertical motion, preventing unrestricted movement in this direction. This factor was not considered in the present study and will be a subject of future research by the authors.

Declaration of competing interest

The authors declare that they have no known competing financial interests or personal relationships that could have appeared to influence the work reported in this paper.

Acknowledgement

The authors gratefully acknowledge the financial support through the Equinor Akademia Program at the University of Stavanger.

Appendix A

Table 10
Eigen periods and eigen vectors of the coupled system for range of sea wave periods (4–21s).

Body	Mode		6	7	8	9	10	11
Barge	Surge	[m]	−0.181	0.006	0.002	0.00	0.00	0.00
Barge	Sway	[m]	0.00	0.00	0.00	0.01	0.00	0.047
Barge	Heave	[m]	0.118	0.142	0.006	0.00	0.00	0.00
Barge	Roll	[deg]	0.011	−0.035	0.042	0.244	0.001	0.259
Barge	Pitch	[deg]	**1.00**	−0.164	−0.016	0.003	0.00	0.00
Barge	Yaw	[deg]	0.02	0.029	−0.032	−0.133	0.00	0.119
Hook	Surge	[m]	0.02	−0.007	0.00	0.00	0.00	0.00
Hook	Sway	[m]	0.113	−0.213	0.225	0.221	0.001	−0.292
Hook	Heave	[m]	**−0.631**	0.271	0.019	−0.004	0.00	0.00
Monopile	Surge	[m]	0.00	0.00	0.00	0.00	0.00	0.00
Monopile	Sway	[m]	0.034	−0.078	0.09	0.373	0.00	−0.315
Monopile	Heave	[m]	**−0.637**	0.273	0.019	−0.003	0.00	0.00
Monopile	Roll	[deg]	**−0.585**	**1.00**	**−1.00**	**1.00**	0.00	−0.134
Monopile	Pitch	[deg]	0.131	−0.057	−0.004	0.00	0.00	0.00
Monopile	Yaw	[deg]	0.052	−0.109	0.123	0.58	**1.00**	**1.00**
	Natural period	[s]	7.139	7.795	8.057	11.543	16.310	20.964

References

Acero, W.G., Gao, Z., Moan, T., 2016a. Assessment of the dynamic responses and allowable sea states for a novel offshore wind turbine installation concept based on the inverted pendulum principle. Energy Proc. 94, 61–71.

Acero, W.G., Li, L., Gao, Z., Moan, T., 2016b. Methodology for assessment of the operational limits and operability of marine operations. Ocean Eng. 125, 308–327.

Baar, J., Pijfers, J., van Santen, J., 1992. Hydromechanically Coupled Motions of a Crane Vessel and a Transport Barge, Offshore Technology Conference. OTC. OTC-6949-MS.

Cadet, O., 2003. Introduction to kalman filter and its use in dynamic positioning systems. Proceedings of Dynamic Positioning Conference, pp. 16–17. Houston, USA.

Chen, K., Zhang, H., Niu, Z., Zhou, L., He, W., Wang, J., 2014. Dynamic responses of a steel cylinder in the process of lifting by a floating crane in waves. International Conference on Offshore Mechanics and Arctic Engineering. American Society of Mechanical Engineers. V01BT01A030.

Chen, M., Yuan, G., Li, C.B., Zhang, X., Li, L., 2022. Dynamic analysis and extreme response evaluation of lifting operation of the offshore wind turbine jacket foundation using a floating crane vessel. J. Mar. Sci. Eng. 10 (12), 2023 ctypes — A Foreign Function Library for Python. (accessed online: 25.11.2024). URL: https://docs.python.org/3/library/ctypes.html.

Chen, M., Yuan, G., Li, B., Li, C.B., Ouyang, M., Li, L., Shi, W., Han, Z., Zhang, W., Chen, Z., 2024. Dynamic analysis of lift-off operation of offshore wind turbine jacket foundation from the transportation barge. Ocean Eng. 301, 117443.

de Andrade, E.M., de Oliveira Costa, D., Fernandes, A.C., Junior, J.S.S., 2023. A review on the modeling of subsea lifting operations. Ocean Eng. 268, 113293.

Deng, Y., Ren, X., Nuernberg, M., Tao, L., 2023. Dynamic analysis of launching and recovering ROV. International Conference on Offshore Mechanics and Arctic Engineering. American Society of Mechanical Engineers. V001T01A024.

Dieseko Group, 2017. Decommissioning Lely Offshore Wind Farm.

DNV, Recommended Practice 2021. (DNV-RP-N103): Modelling and Analysis of Marine Operations.

DNV GL-CG-0130, 2018. Wave Loads - Rules and Standards. Edition January.

Fossen, T.I., Perez, T., 2009. Kalman filtering for positioning and heading control of ships and offshore rigs. IEEE Control Syst. Mag. 29 (6), 32–46.

Gao, L., Liu, T., Halse, K.H., Jiang, Z., 2023. Numerical analysis of the offshore wind turbine pre-mating process using a low-height lifting system for a nonconventional installation vessel. Ocean Eng. 286, 115555.

GitHub - SINTEF/simapy. Python API to interact with SIMA (accessed online. https://github.com/SINTEF/simapy. (Accessed 15 March 2024).

Gordon, R.B., Grytøyr, G., Dhaigude, M., 2013. Modeling suction pile lowering through the splash zone. International Conference on Offshore Mechanics and Arctic Engineering. American Society of Mechanical Engineers. V001T001A010.

Hinzmann, N., Gattermann, J., Lehn, P., 2020. Large-scale tests with hydraulic and pneumatic overpressure for monopile decommissioning of offshore wind turbines. In: International Conference on Offshore Mechanics and Arctic Engineering, vol. 84423. American Society of Mechanical Engineers. V010T10A012.

Hinzmann, N., Lehn, P., Gattermann, J., 2021. Large-scale model investigation for monopile decommissioning of offshore wind turbines: overpressure and vibratory pile. In: International Conference on Offshore Mechanics and Arctic Engineering, vol. 84768. American Society of Mechanical Engineers. V001T02A003.

Hong, S., Zhang, H., Nord, T.S., Halse, K.H., 2022. Effect of fender system on the dynamic response of onsite installation of floating offshore wind turbines. Ocean Eng. 259, 111830.

Hong, S., Zhang, H., Halse, K.H., 2023. Hydrodynamic and environmental modelling influence on numerical analysis of an innovative installation method for floating wind. Ocean Eng. 280, 114681.

Komusanac, I., Brindley, G., Fraile, D., Ramirez, L., 2022. Wind Energy in Europe–2021 Statistics and the Outlook for 2022–2026. WindEurope, Brussels, Belgium, p. 37.

Li, L., Gao, Z., Moan, T., Ormberg, H., 2014. Analysis of lifting operation of a monopile for an offshore wind turbine considering vessel shielding effects. Mar. Struct. 39, 287–314.

Li, L., Gao, Z., Moan, T., 2015a. Comparative study of lifting operations of offshore wind turbine monopile and jacket substructures considering vessel shielding effects.

ISOPE International Ocean and Polar Engineering Conference. ISOPE. ISOPE-I-15-084.
Li, L., Gao, Z., Moan, T., 2015b. Response analysis of a nonstationary lowering operation for an offshore wind turbine monopile substructure. J. Offshore Mech. Arctic Eng. 137 (5), 051902.
Li, L., Guachamin Acero, W., Gao, Z., Moan, T., 2016. Assessment of allowable sea states during installation of offshore wind turbine monopiles with shallow penetration in the seabed. J. Offshore Mech. Arctic Eng. 138 (4), 041902.
Li, B., Qiao, D., Zhao, W., Hu, Z., Li, S., 2022. Operability analysis of SWATH as a service vessel for offshore wind turbine in the southeastern coast of China. Ocean Eng. 251, 111017.
Microsoft documentation. Introduction to Dynamic-Link Libraries (DLLs) (accessed online: 25.November.2024). https://learn.microsoft.com/en-us/windows/win32/dlls/dynamic-link-libraries.
Salahshour, S., Ong, M.C., Skaare, B., Jiang, Z., 2022. A perspective of decommissioning methods for bottom-fixed offshore wind turbines. International Conference on Offshore Mechanics and Arctic Engineering. American Society of Mechanical Engineers. V008T009A058.
Salahshour, S., Ong, M.C., Nematzadeh, A., 2023. Numerical study on vibratory extraction of offshore wind turbine monopile foundations under sandy seabed condition. Ocean Eng. 289, 116229.
Salahshour, S., Janbazi, H., Ong, M.C., 2024. Numerical modelling of vibratory extraction of monopiles from clayey seabed. Ocean Eng. 297, 117155.
Shafiee, M., Adedipe, T., 2022. Offshore wind decommissioning: an assessment of the risk of operations. Int. J. Sustain. Energy 41 (8), 1057–1083.
SIMA Documentation https://sima.sintef.no/doc/4.8.0/simo/index.html.
Van Doorn, N., 2016. Environmental Limitations in Suction Bucket Based Jacket Foundation Installation, Using Vertical Lift-Off from a Jack-Up Vessel.
van Dorp, R., Middendorp, P., Bielefeld, M., Verbeek, G., 2021. Decommissioning offshore structures by extraction of foundation mono piles applying a vibratory hammer. Offshore Technology Conference. OTC. D041S051R003.
Zhang, P., Ding, H., Le, C., 2022a. Response analysis of a lowering operation for a three-bucket jacket foundation for offshore wind turbines. Renew. Energy 185, 564–584.
Zhang, P., Zhang, S., Wei, Y., Le, C., Ding, H., 2022b. Hydrodynamic characteristics of the crane vessel-three-bucket jacket foundation coupling hoisting system during the process of lowering. Ocean Eng. 250, 111034.
Zhao, Y., Cheng, Z., Sandvik, P.C., Gao, Z., Moan, T., 2018. An integrated dynamic analysis method for simulating installation of single blades for wind turbines. Ocean Eng. 152, 72–88.
Zhu, H., Li, L., Ong, M., 2017. Study of lifting operation of a tripod foundation for offshore wind turbine. IOP Conference Series: Materials Science and Engineering. IOP Publishing, 012012.